Epigenetic modulation extends the oncogene addiction paradigm on the basis of tumor cell differentiation state

Mehwish Khaliq [1,2], Mohan Manikkam [1], Elisabeth D. Martinez [3,4], and Mohammad Fallahi-Sichani [1,5]

[1] Department of Biomedical Engineering, University of Michigan Medical School, Ann Arbor, MI

[2] Program in Cancer Biology, University of Michigan Medical School, Ann Arbor, MI

[3] Department of Pharmacology, UT Southwestern Medical Center, Dallas, TX

[4] Hamon Center for Therapeutic Oncology Research, UT Southwestern Medical Center, Dallas, TX

[5] Department of Biomedical Engineering, University of Virginia, Charlottesville, VA

Address correspondence to:

Mohammad Fallahi-Sichani

Address: 415 Lane Rd, Building MR5, Room 2115, Charlottesville, VA 22903

ORCID ID: 0000-0003-0917-3525

Tel/Fax: (434) 924-9950

Email: fallahi@virginia.edu

Abstract

The hyperactivation of MAPK signaling pathway motivates the clinical use of MAPK inhibitors to treat BRAF-mutant melanomas. Heterogeneity in differentiation state due to epigenetic plasticity, however, results in cell-to-cell variability in the state of MAPK dependency and diminishes the efficacy of MAPK inhibitors. To identify key regulators of such variability and potential mitigation strategies, we screened 276 epigenetic-modifying compounds, individually and in combination with MAPK inhibitors, across both genetically distinct and isogenic populations of melanoma cells. Integrated with single-cell analysis and multivariate modeling, we identified three classes of epigenetic inhibitors that target seemingly distinct epigenetic states associated with either one of the lysine-specific histone demethylases KDM1A, or KDM4B, or BET bromodomain proteins. While melanocytes remained insensitive, the anti-tumor efficacy of each inhibitor was predicted based on a melanoma cell's differentiation state and MAPK activity. Our systems pharmacology approach highlights an avenue toward identifying actionable epigenetic factors that extend the BRAF oncogene addiction paradigm on the basis of tumor cell differentiation state.

Introduction

The discovery of driver oncogenes has revolutionized drug development strategies for an increasing number of cancers. Despite great promise, however, therapeutic inhibition of oncogenic signaling often leads to variable response rates due to cell-to-cell heterogeneity in the state of oncogene dependency [1]. Such heterogeneity may result from secondary genetic mutations. In many cases, however, it cannot be linked to a clear genetic cause, but rather appears to be associated with epigenetic factors established by a cell's developmental lineage or differentiation state [2–10]. A paradigmatic example of epigenetic heterogeneity in the state of oncogene dependency is observed among melanomas that carry V600E/D/K mutations in the BRAF oncogene. Despite dramatic responses, BRAF/MEK targeted therapies often fail to eradicate BRAF-mutant melanoma cells [11]. Drug resistance usually arises following fractional responses associated with either the enrichment of a subpopulation of drug-tolerant cells that are intrinsically insensitive to the effect of BRAF/MEK inhibition, or the acquisition of adaptive phenotypes with reversibly reduced dependency on MAPK signaling [12–22].

Numerous studies have associated such fluctuations in the state of MAPK pathway dependency (which arise even among isogenic cells [23]) to melanoma differentiation state plasticity [6,19,24–27]. Such plasticity spans a spectrum, ranging from a pigmented melanocytic phenotype associated with master transcriptional regulators SOX10 and MITF (i.e. $MITF^{High}$ state) [28], to a neural crest-like state that expresses NGFR (i.e. $NGFR^{High}$ state) [13,29], to an undifferentiated state characterized by high expression of receptor tyrosine kinases such as AXL (i.e. AXL^{High} state) [20,30]. Melanoma tumors consist of a mixture of these phenotypes at variable single-cell frequencies [25]. Although the consequences of such epigenetic heterogeneities for drug resistance are widely recognized, there is still little known about actionable epigenetic factors that may link heterogeneity in the state of MAPK dependency to plasticity in differentiation state. A system-wide exploration of these factors may reveal novel opportunities for

epigenetic treatments that will minimize the emergence of drug resistance. In principle, identifying epigenetic treatments that promote cellular requirement for MAPK signaling may enhance the efficacy of BRAF/MEK inhibitors when used in combination [13,31–33]. Alternatively, treatments that target synthetic lethal partners of the BRAF oncogene, in a specific epigenetic context or differentiation state, may serve as a possible strategy to selectively kill drug-resistant cells [34].

In this paper, we took a systems pharmacology approach to test the hypothesis that heterogeneity in the state of MAPK pathway dependency may result from a subset of key epigenetic variations across tumor cells of heterogeneous differentiation states. To identify regulator of such variations, we used a library of 276 small molecule epigenetic modulators in BRAF-mutant cell lines that cover a wide spectrum of melanoma differentiation states. We performed a systematic analysis of the effect of each epigenetic modulator (assayed individually and in combination with BRAF and MEK kinase inhibitors) on melanoma cell survival, proliferation, differentiation state, activity of the MAPK signaling pathway, and their variations with treatment dose and time. Integrating multiplexed single-cell analysis of a panel of 16 cell lines with multivariate statistical modeling and genetic experiments, we identified three classes of small molecules that target seemingly distinct epigenetic states in melanoma cells. These epigenetic states included: (i) a lysine demethylase 1A (KDM1A)-dependent state, predominantly observed in undifferentiated (AXL^{High}), BRAF/MEK inhibitor-resistant ($p\text{-}ERK^{High}$) cells, that is efficiently inhibitable by the reversible KDM1A inhibitor SP2509 (and its clinical formulation SP2577; Seclidemstat), (ii) a lysine demethylase 4B (KDM4B)-dependent state, associated with neural crest-like ($NGFR^{High}/AXL^{Low}$) cells, that is sensitive to JIB-04 (a pan-inhibitor of Jumonji histone demethylases) and induces synergistic cell death upon exposure to the combination of JIB-04 and BRAF/MEK inhibitors, and (iii) a state induced by BET bromodomain inhibitors such as OTX015 (Birabresib) in $NGFR^{High}$ cells, which substantially enhances their requirement for MAPK signaling and, thereby, their

sensitivity to BRAF/MEK inhibitors. Single-cell analysis of tumor lines shows that these states might co-exist in different combinations and frequencies, highlighting mutual epigenetic vulnerabilities among genetically diverse melanoma cell populations. Importantly, non-transformed primary melanocytes were not sensitive to any of the identified epigenetic inhibitors. These results, therefore, provide a framework for the identification of actionable epigenetic factors that may extend the oncogene addiction paradigm on the basis of melanoma differentiation state.

Results

Single-cell analysis uncovers heterogeneities in melanoma differentiation, proliferation and MAPK signaling states

To elucidate single-cell heterogeneities in differentiation state and their variations across genetically diverse melanoma cell populations and BRAF/MEK inhibitor treatment conditions, we utilized high-throughput, multiplex immunofluorescence microscopy. A panel of sixteen $BRAF^{V600E/D}$ melanoma cell lines and a batch of non-transformed human primary epidermal melanocytes were exposed to the BRAF inhibitor vemurafenib (at 100 nM), alone or in combination with the MEK inhibitor trametinib (at 10 nM). Cells were fixed following 3 to 5 days of treatment and protein levels of three differentiation state markers, MITF, NGFR and AXL, were quantified at a single-cell level. To visualize baseline and treatment-induced single-cell heterogeneities in a two-dimensional space, we performed *t*-distributed stochastic neighbor embedding (t-SNE) analysis on a total population of 6069 randomly selected cells from all of the 102 tested conditions, covering the entire panel of cell lines, drugs and timepoints (Fig. 1a). Single-cell analysis revealed a continuum of differentiation states ranging from $MITF^{High}$ (highly differentiated) to $NGFR^{High}$ (neural crest-like) to AXL^{High} (undifferentiated) cells. In agreement with previous reports, cells expressing very high levels of any one differentiation marker typically expressed

low levels of the other two markers. Interestingly, however, some cells projected along transitory states, expressing moderate levels of more than one marker (e.g. MITF and NGFR or NGFR and AXL), which might be explained by previously observed transient fluctuations between these states [13,23]. Using the t-SNE map as a reference, we analyzed the baseline differentiation state and treatment-induced changes in the behavior of isogenic cell populations from each cell line (Fig. 1b). All clonal cell lines (except for LOXIMVI) exhibited highly heterogenous populations, expressing substantial plasticity following exposure to vemurafenib or its combination with trametinib. Surprisingly, non-transformed melanocytes also exhibited heterogeneity at a level comparable to melanoma cell lines, suggesting that plasticity in differentiation state is not unique to cancer cells.

Because proliferation of BRAF-mutant cells is attributed to their aberrant MAPK signaling, we next asked whether heterogeneity in melanoma differentiation state was associated with potentially distinct patterns in MAPK signaling and cellular proliferation following BRAF/MEK inhibition. To address this question, we first multiplexed single-cell immunofluorescence measurements of p-ERK$^{T202/Y204}$, Ki-67 (a proliferation marker), and p-S6$^{S235/S236}$ (a marker of TORC1 activity, downstream of both ERK and the parallel PI3K/AKT pathways, and one of the best predictors of which is commonly up-regulated in MAPK inhibitor-tolerant cells [35]) in the same group of cell lines exposed to the same BRAF/MEK inhibitors for 3 to 5 days. Single-cell analysis by t-SNE revealed a trajectory along which cells were clustered on the basis of their p-ERK, p-S6 and Ki-67 levels (Fig. 1c). The distribution of cells along this trajectory depended on the extent of the MAPK pathway inhibition by each drug. Vemurafenib-treated cells (Fig.1d; yellow circles) exhibited a heterogeneous response with only partial inhibition of MAPK signaling relative to drug-naïve (p-ERK^{High}/p-S6^{High}/Ki-67^{High}) cells (Fig 1d; gray circles). The combination of vemurafenib and trametinib (Fig 1d; red circles) suppressed the MAPK pathway more strongly and drove a larger proportion of cells toward a fully inhibited (p-ERK^{Low}/p-

S6^{Low}/Ki-67^{Low}) state. The fraction of fully inhibited cells, however, varied among different cell lines. We hypothesized that such variability in MAPK signaling would explain differences in the overall MAPK inhibitor sensitivity and might be linked to heterogeneity in melanoma differentiation state.

To compare overall BRAF/MEK inhibitor sensitivity among cell lines while correcting for differences in their baseline proliferation rates, we first calculated the average net growth rates from time-dependent changes in live cell counts following exposure of each cell line to drugs or DMSO (Fig. 1e and Supplementary Fig. 1a). Drug-induced normalized growth rates (i.e. DIP rates [36]) were then computed by normalizing the average net growth rate in the presence of each drug (i.e. vemurafenib alone, or vemurafenib in combination with trametinib) to that in DMSO-treated cells (Fig. 1f). Normalized growth rates < 0 indicated a net cell loss (i.e. cytotoxicity), a value of 0 represented no change in viable cell number (i.e. cytostasis), a value > 0 indicated a net cell gain (i.e. population growth), and a value of 1 represented cell growth at the same rate as in DMSO-treated (control) cells. By correlating drug-induced normalized growth rates to the state of MAPK signaling across 16 cell lines, we identified a strong correlation between the fraction of fully inhibited (p-ERK^{Low}/p-S6^{Low}/Ki-67^{Low}) cells and the overall (population-average) sensitivity to BRAF/MEK inhibitors (Pearson's r = -0.65, P = 4.3×10^{-9}) (Supplementary Fig. 1b and Fig. 1g; top left panel). We next extended the systematic correlation analysis to the diversity of differentiation states. We discovered that upon BRAF/MEK inhibition, predominantly undifferentiated (AXL^{High}) cell lines generated the smallest populations of fully inhibited cells (Supplementary Fig. 1b and Fig. 1g; top right panel). BRAF/MEK inhibitor resistance in these cells was associated with a high frequency of proliferating (Ki-67^{High}) cells exhibiting incomplete inhibition of the MAPK pathway. In contrast, populations of neural crest-like (NGFR^{High}/AXL^{Low}) cells or differentiated (MITF^{High}) cells exhibited substantial co-inhibition of p-ERK, p-S6 and Ki-67 (Supplementary Fig. 1b and Fig. 1g; bottom panels). Drug adaptation in these

populations was, therefore, associated with an overall reduced requirement for MAPK signaling.

Together, these analyses revealed a spectrum of heterogeneities in melanoma differentiation state that corresponded to two previously described and distinct ways through which cells may tolerate the effect of BRAF/MEK inhibition: (1) incomplete inhibition of the MAPK pathway (as seen in AXL^{High} cells), and (2) reduced requirement for MAPK signaling (as seen predominantly in $NGFR^{High}/AXL^{Low}$ cells). Next, we asked whether there are epigenetic features associated with each melanoma differentiation state that might be exploited to overcome either of these drug tolerance mechanisms.

A chemical screen identifies epigenetic modulators of phenotypic heterogeneity

To systematically search for epigenetic factors that may link heterogeneity in melanoma differentiation state to MAPK dependency, we performed a multi-stage phenotypic screen using a library of 276 epigenetic modifying compounds. Each compound was used to modulate either a key epigenetic writer, eraser or reader, or a related protein, after which phenotypic responses in the presence or absence of BRAF/MEK inhibitors were investigated. For the first stage of the compound screen, we selected COLO858 and MMACSF cell lines based on their heterogeneous differentiation and MAPK signaling states in response to BRAF/MEK inhibitors (Fig. 2a). We hypothesized that such heterogeneity would facilitate our search for compounds that target diverse mechanisms of drug tolerance, MAPK dependency and epigenetic heterogeneity. To test this hypothesis, cells from both cell lines were initially exposed to two different doses (0.2 and 1 μM) of each of the 276 epigenetic compounds or vehicle (DMSO) for 24 h. Vemurafenib alone (at 100 nM), vemurafenib in combination with trametinib (at 10 nM), or vehicle (DMSO), was then added and cells were grown for a further 72 or 120 h prior to fixation (Fig. 2b). To differentiate the impact of epigenetic compounds, the growth rates for cells treated with each epigenetic compound were normalized to cells treated without any epigenetic compound for each

treatment condition (i.e., DMSO, vemurafenib, and vemurafenib plus trametinib). Statistical analysis identified 58 compounds that led to a significant decrease in normalized growth rate in at least one of the tested conditions (Supplementary Fig. 2 and 3).

To infer potential variations in the mechanisms of action of the epigenetic compounds, we co-stained cells for p-ERK$^{T202/Y204}$, p-Rb$^{S807/811}$, and MITF, quantifying changes induced by each of the 58 compounds on MAPK signaling, cell cycle progression, and differentiation state, respectively. Unsupervised clustering of the normalized responses revealed remarkable similarities among groups of distinct compounds with common nominal epigenetic targets, suggesting that these responses are most likely the consequence of their on-target effects (Fig. 2c and Supplementary Fig. 4a). These compounds comprised of BET bromodomain inhibitors, lysine demethylase 1A (KDM1A) inhibitors, a pan-inhibitor of the Jumonji family of lysine demethylases (Jmj-KDMs), Tankyrase inhibitors, Aurora kinase inhibitors, and two distinct groups of histone deacetylase (HDAC) inhibitors. Each class of compounds induced distinct phenotypic responses that were either cell line- or MAPK inhibitor-specific, or common between both cell lines, or independent of MAPK inhibitor condition. For example, CUDC-907 (Fimepinostat), Quisinostat, Panobinostat, Dacinostat, and Trichostatin A were identified as a cluster of HDAC inhibitors (labeled as group 1 in Fig. 2c) that significantly reduced growth rate in both COLO858 and MMACSF cells to similar degrees and independent of MAPK inhibitor conditions (Supplementary Fig. 4a,b). In contrast, KDM1A inhibitors inhibited net growth rate selectively in COLO858 cells, and they showed a higher efficacy in the absence of BRAF/MEK inhibitors.

Correlated patterns of melanoma responsiveness to mechanistically distinct epigenetic inhibitors

To identify potential relationships between the efficacy of each class of epigenetic compounds, we sought to analyze their effects (individually and in combination with BRAF/MEK inhibitors) across a

more diverse group of cell lines. Thus, in the second stage of our screen, we focused on seven epigenetic inhibitors representing the most effective classes identified in the first stage (including HDAC inhibitors CUDC-907 and Givinostat, pan-Jmj-KDM inhibitor JIB-04, Tankyrase inhibitor AZ6102, BET inhibitors I-BET762 and OTX015 (Birabresib), and KDM1A inhibitor SP2509) and a group of eight cell lines representing a larger spectrum of differentiation states (Fig. 3a,b). By testing each compound in non-transformed human primary melanocytes, we chose effective concentrations of each inhibitor that had little to no effect on healthy cells (Supplementary Fig. 5). To quantify the benefit resulting from combining each of the epigenetic inhibitors with MAPK inhibitors, we computed drug combination index (CI) values based on the difference between the effect of combination treatment (i.e. normalized growth rate in the presence of epigenetic inhibitor plus MAPK inhibitors) and that of the most efficacious individual treatment (i.e. the smaller of the normalized growth rates between epigenetic inhibitor and MAPK inhibitor treatments) (Fig. 3c). This is consistent with a framework proposed by Gaddum [37] (also known as the Highest Single Agent model), where any combined effect stronger than a single drug (CI < 0) is called synergism, any effect weaker than a single drug (CI > 0) is called antagonism, and a combined effect exactly equal to the strongest single drug (CI = 0) shows the dominance of one drug relative to the other one. Similar to our previous observations in COLO858 and MMACSF cells, we found that the HDAC inhibitor CUDC-907 induced substantial tumor cell killing in the rest of the six melanoma cell lines tested. CUDC-907 was not only effective as a single-agent, but also exhibited a synergistic response in combination with BRAF/MEK inhibitors. Treatment with the other six compounds, however, uncovered cell line-specific and MAPK inhibitor-dependent patterns. For example, BET inhibitors OTX015 and I-BET762 both induced a strong cytotoxic effect only in four of the tested cell lines (MMACSF, COLO858, WM115 and A375) and only after those cell lines were exposed to the triple combination of BET inhibitor plus vemurafenib and trametinib. The combination of

BET inhibitors with BRAF/MEK inhibitors was, therefore, cell line-specific and synergistic.

To systematically explore the patterns of melanoma cell responses to epigenetic inhibitors, we computed all pairwise correlations between the efficacy of seven epigenetic compounds (alone and in combination with BRAF/MEK inhibitors) across the eight cell lines (Fig. 3d). As expected, the efficacy of two BET inhibitors, OTX015 and I-BET762, was strongly correlated (Pearson's $r = 0.99$, $P < 10^{-4}$). In addition, the efficacy of BET inhibitors and the pan-Jmj-KDM inhibitor JIB-04 was significantly and positively correlated when cells were co-treated with vemurafenib plus trametinib ($r = 0.85$, $P < 10^{-3}$). In contrast, a significant but negative correlation was observed between the efficacies of JIB-04 and the KDM1A inhibitor SP2509.

Next, we focused on epigenetic compounds (OTX015, I-BET762, JIB-04 and SP2509) exhibiting correlated patterns of response across the eight cell lines and asked whether such correlations would be maintained if these compounds were assayed across a larger panel of melanoma cell lines. By expanding the analysis to a total of sixteen cell lines, we confirmed the statistical significance of the negative correlation between responses to SP2509 and JIB-04 (Fig. 4a). In more than half of the cell lines tested, five days of treatment with SP2509 induced substantial cell killing (Fig. 4b and Supplementary Fig. 6a). SP2509 sensitivity correlated with sensitivity to SP2577 (seclidemstat; a clinical formulation of SP2509), which also suppressed melanoma cell growth (when used at a daily dose of 80 mg/kg) in corresponding melanoma xenografts (Supplementary Fig. 6b-d). Interestingly, however, cell lines with the highest level of resistance to SP2509 and SP2577 were sensitive to JIB-04, showing a range of responses from cytostatic to cytotoxic (Fig. 4a-c, Supplementary Fig. 6a). The triple combination of JIB-04, vemurafenib and trametinib was highly cytotoxic, inducing synergistic cell killing in all JIB-04-sensitive cell lines, whereas the combination of SP2509 with BRAF/MEK inhibitors did not result in an additional benefit in most cell lines (Fig. 4c). When combined with vemurafenib and

trametinib, both BET inhibitors OTX015 and I-BET762 also induced synergistic cell killing in most of the JIB-04-sensitive cell lines, while having minimal effects (0 << normalized growth rate ≤ 1) when used as a single agent in those cell lines. To determine if the epigenetic inhibitor effects were transient or persisted with long-term exposure, we extended the duration of growth assays up to 20 days post-treatment (Fig. 4d). We found that the optimal epigenetic treatments identified for three of the MAPK inhibitor-resistant cell lines were highly efficacious in time, resulting in continuous cell killing and a reduction of up to ~1000 fold in live cell count over a period of 20 days.

Together, our multi-stage epigenetic screen and systematic analysis identified a set of seemingly distinct epigenetic states whose inhibition, either by the KDM1A inhibitor SP2509 (as a single-agent), or by the pan-Jmj-KDM inhibitor JIB-04 or BET inhibitors OTX015 and I-BET762 (when used in combination with BRAF/MEK inhibitors), led to tumor cell killing in a melanoma cell line-specific manner. Next, we asked whether distinctive patterns of melanoma cell responses to these inhibitors may be linked to the heterogeneity present in their MAPK signaling, proliferation or differentiation states.

Multivariate modeling identifies differentiation state-specific predictors of epigenetic inhibitor efficacy

To systematically determine whether molecular markers of melanoma differentiation state, MAPK signaling activity or other phenotypic markers could predict the differential efficacy of epigenetic treatments, we measured both baseline levels and treatment-induced variations in MITF, NGFR, AXL, SOX10, p-ERK$^{T202/Y204}$, p-S6$^{S235/S236}$ and Ki-67 across eight melanoma cell lines. Given the possible contribution of epigenetic histone modifications in DNA damage repair [38], we also included phosphorylated Histone p-H2A.X^{S139} (a marker of DNA damage response) in our analysis. Multiplexed immunofluorescence measurements revealed how multiple signaling proteins and phenotypic markers

were up- or down-regulated depending on the cell line, MAPK inhibitor condition and epigenetic treatment (Fig. 5a). We then used partial least square regression (PLSR) analysis [39] to generate models that linked epigenetic treatment-induced changes in growth rates ("response" variables) to "input" vectors that combined baseline and treatment-induced changes in signaling and phenotypic data. Models were evaluated by computing the correlation between measured and predicted responses using leave-one-out cross-validation (Supplementary Fig. 7a). Overall, PLSR models built for JIB-04, SP2509, I-BET762 and OTX015 proved remarkably accurate with an average Pearson's correlation coefficient of 0.85 ± 0.06 (for three PLSR components) (Fig. 5b and Supplementary Fig. 7b). High performance of PLSR models demonstrated that variations in at least some of the measurements could explain the variability in growth rate by each of these epigenetic compounds.

To identify those measurements that are predictive of epigenetic treatment efficacy, we computed the Variable Importance in the Projection (VIP) scores for each PLSR model [40]. VIP analysis made it possible to visualize combinations of measurements, and changes induced by each epigenetic compound, that were predictive of their efficacy in tumor cell killing (Fig. 5c and Supplementary Fig. 7c). Among the most important determinants of treatment efficacy were differentiation markers AXL and NGFR as well as measurements of MAPK activity, including p-ERK, p-S6 and Ki-67. Informed by the PLSR results, single-cell analysis across the entire panel of cell lines showed that SP2509 was most effective (when used as a single agent) in inhibiting AXL^{High} populations of cells that were intrinsically insensitive to BRAF/MEK inhibitors (Fig. 5d and Supplementary Fig. 7d). In contrast, $NGFR^{High}/AXL^{Low}$ populations exhibited a highly synergistic response to the combination of JIB-04 with vemurafenib plus trametinib (Fig. 5d and Supplementary Fig. 7d). Additionally, BET inhibitors I-BET762 and OTX015 (when combined with BRAF/MEK inhibitors) enhanced tumor cell killing most significantly in populations of $NGFR^{High}$ (or $MITF^{Low}/AXL^{Low}$) cells (Supplementary Fig. 7d).

Together, these data reveal how distinctive patterns of responsiveness to SP2509, JIB-04 and BET inhibitors (individually or in combination with BRAF/MEK inhibitors) are linked to the state of MAPK signaling and differentiation state. Cells in undifferentiated (AXL^{High}) and neural crest-like ($AXL^{Low}/NGFR^{High}$) states represent two different forms of drug tolerance observed at variable frequencies across most melanoma tumors. Their selective sensitivity to the identified epigenetic inhibitors, therefore, supports the hypothesis that there are epigenetic features associated with melanoma differentiation state that may be exploited to overcome diverse mechanisms of MAPK inhibitor resistance.

KDM protein levels determine differentiation state-specific sensitivity to KDM inhibitors

Our epigenetic compound screen and subsequent analyses revealed melanoma differentiation state as a major predictor of the efficacy of lysine-specific demethylase (KDM) inhibitors, JIB-04 and SP2509, in melanoma cells. These compounds inhibit structurally distinct histone demethylases that are expressed collectively at a higher level in melanoma tumors relative to primary melanocytes [34]. We thus sought to utilize our knowledge of interactions between these compounds and their protein targets to better understand the origins of their selective efficacy in melanoma cells.

JIB-04 has been previously characterized as a pan-inhibitor of Jmj-KDMs, suppressing the activities of KDM4A, KDM4B, KDM5A and KDM5B, all with IC_{50}'s < 0.5 μM, while having no significant effect on the structurally unrelated demethylases such as KDM1A [41]. We thus asked which of the Jmj-KDM proteins targeted by JIB-04 might explain its synergistic effect with the combination of BRAF/MEK inhibitors in BRAF-mutant melanoma cells. To address this question, we examined the correlation between drug combination index for JIB-04 plus vemurafenib and trametinib and protein levels of each of the JIB-04 targets, KDM4A, KDM4B, KDM5A and KDM5B. In nine of our melanoma

cell lines, for which quantitative proteomics data from the Cancer Cell Line Encyclopedia (CCLE) [42] are available, the KDM4B protein level was the most significant predictor of JIB-04 efficacy (Fig. 6a). Furthermore, KDM4B protein levels were highest in melanoma cell lines that expressed a neural crest-like phenotype and high levels of NGFR relative to AXL (Fig. 6b).

To directly test whether selective inhibition of KDM4B can suppress the survival of JIB-04-sensitive melanoma cells, we depleted KDM4A, KDM4B, KDM5A and KDM5B by siRNA in two JIB-04-sensitive cell lines, WM115 and WM902B, and in a JIB-04-resistant cell line, A2058 (Supplementary Fig. 8a). Only depletion of KDM4B in WM115 and WM902B cells, but not in A2058 cells, led to a statistically significant decrease in live cell count and enhanced their sensitivity to the combination of vemurafenib and trametinib (Fig. 6c). A2508 cells were, however, sensitive to KDM1A knockout by CRISPR (Supplementary Fig. 8b and Fig. 6d), which correlated with their sensitivity to KDM1A inhibitor SP2509. SP2509 acts as an allosteric inhibitor, blocking KDM1A interaction with its coactivator, Zinc Finger Protein 217 (ZNF217) [43]. In agreement with its mechanism of action, SP2509 efficacy was significantly greater in melanoma cell lines, in which KDM1A and ZNF217 proteins were expressed collectively at a higher level (Fig. 6e). Cell lines expressing higher levels of KDM1A and ZNF217 also expressed AXL at a significantly higher level (Fig. 6f). Together, these results demonstrate that the relative levels of KDM4B protein and KDM1A plus ZNF217 proteins, can predict the differentiation state-specific sensitivity of melanoma cells to JIB-04 and SP2509.

Discussion

Growing evidence suggests that lineage-specific epigenetic mechanisms and their reprograming following oncogene inhibition may generate drug-tolerant states that diminish the efficacy of targeted therapies [44]. In BRAF-mutant melanomas, comparable states tolerant of MAPK pathway inhibition have

been associated with variations in differentiation state, represented by levels of SOX10, MITF, NGFR and receptor tyrosine kinases such as AXL. Through high-throughput profiling of a panel of human melanoma cell lines, we observed recurrent patterns of single-cell heterogeneity in differentiation state comparable to those previously seen in patient tumors [25]; each tumor line consisted of a mixture of cells at diverse differentiation states with single-cell frequencies that varied from one genotype to another. We found that a melanoma cell's ability to tolerate the effect of BRAF/MEK inhibition was correlated with its differentiation state. Responses of undifferentiated (AXL^{High}) cells, for example, were associated with incomplete inhibition of the MAPK pathway, whereas MAPK-inhibited neural crest-like ($NGFR^{High}/AXL^{Low}$) cells adapted to BRAF/MEK inhibitor treatment by reducing their requirement for MAPK signaling. Because neither of the differentiation state markers are ideal therapeutic targets, we hypothesized that variability in BRAF/MEK inhibitor sensitivity may be overcome via targeting epigenetic features that are linked to specific melanoma differentiation states.

In this study, we combined high-throughput screening, multiplexed protein measurements, single-cell analysis, and multivariate modeling, to identify three classes of compounds that target seemingly distinct epigenetic features associated with either one of the lysine-specific histone demethylases KDM1A or KDM4B, or BET proteins in melanoma cells. While non-transformed melanocytes remained unaffected by these compounds, their efficacy in melanoma cells depended on a cell's state of MAPK activity and differentiation state. The KDM1A inhibitor SP2509 was most effective in inhibiting undifferentiated (AXL^{High}) populations of cells that were intrinsically insensitive to BRAF/MEK inhibitors, whereas the combination of SP2509 with BRAF/MEK inhibitors did not result in an additional benefit and even showed some level of antagonism. This is consistent with a recent finding regarding a role that KDM1A plays in disabling $BRAF^{V600E}$ oncogene-induced senescence, thereby promoting BRAF-driven melanogenesis [34]. KDM1A inhibition in the presence of

MAPK signaling may, therefore, restore senescence in AXL^{High} drug-resistant cells. In contrast, neural crest-like ($NGFR^{High}/AXL^{Low}$) populations of cells exhibited a highly synergistic response to the combination of KDM4B inhibition and BRAF/MEK inhibition. BET inhibitors also had minimal effect on melanoma cells when used as a single agent but when combined with BRAF/MEK inhibitors, they led to dramatic tumor cell killing in $NGFR^{High}$ cells. Our systematic studies, therefore, extend previous findings about the potential of each of the epigenetic regulators, KDM1A, Jmj-KDMs and BET proteins, as therapeutic vulnerabilities in melanomas [21,34,45] in two complementary ways. First, by associating these vulnerabilities to the patterns of single-cell heterogeneity in differentiation state, we explain how they may vary from one tumor to another. Second, by linking epigenetic vulnerabilities to the state of BRAF/MAPK dependency, we determine whether each epigenetic inhibitor reaches its maximal efficacy when used as a single agent or when combined with BRAF/MEK inhibitors. Future work will determine the specific mechanisms through which inhibition of each regulator induces melanoma cell killing, and whether we can leverage the combination of epigenetic treatments to increase tumor cell killing in heterogeneous tumors.

Cell-to-cell heterogeneity in the state of oncogene dependency poses a major challenge to the use of targeted therapies across a variety of cancers. A mechanistic understanding of how an oncogenic alteration promotes pathway dependency in tumor cells of a particular differentiation state but not another remains elusive. Our systems pharmacology approach provides a promising avenue toward the identification of actionable epigenetic factors that may extend the oncogene addiction paradigm on the basis of tumor cell differentiation state. We demonstrate the utility of this approach in BRAF-mutant melanomas by using JIB-04 and SP2509, as investigational tools, to block epigenetically diverse populations of MAPK inhibitor-tolerant cells. We show that the relative protein levels of KDM4B and KDM1A plus its coactivator (ZNF217), determine differentiation state-specific sensitivity of melanoma

cells to their corresponding inhibitors. Future work may gauge the mechanistic relationship between the activity of these histone demethylases and melanoma differentiation state at a single-cell level.

Methods

Cell lines and reagents

BRAF-mutant melanoma cell lines used in this study were obtained from the following sources: COLO858 (from ECACC), RVH421 (from DSMZ), A375, A375(NRAS^{Q61K}), C32, A2058, WM115, SKMEL28, HS294T, WM1552C and human adult primary epidermal melanocytes (all from ATCC), LOXIMV1 (from DCTD Tumor Repository, National Cancer Institute), MMACSF (RIKEN BioResource Center), WM902B and WM2664 (from Wistar Institute), UACC62 and SKMEL19 (from the Cancer Cell Line Encyclopedia). All of the cell lines have been periodically subjected to re-confirmation by Short Tandem Repeat (STR) profiling by ATCC and mycoplasma testing by MycoAlert^{TM} PLUS mycoplasma detection Kit (Lonza). A375, A375(NRAS^{Q61K}), A2058 and HS294T cells were grown in DMEM with 4.5 g/l glucose (Corning, Cat# 10-013-CV) supplemented with 5% fetal bovine serum (FBS). C32, MMACSF, SKMEL28 and WM115 cells were grown in DMEM/F12 (Gibco, Cat# 11330-032) supplemented with 1% Sodium Pyruvate (Invitrogen) and 5% FBS. COLO858, LOXIMVI, RVH421, SKMEL19, UACC62, WM1552C and WM902B cells were grown in RPMI 1640 (Corning, Cat# 10-040-CV) supplemented with 1% Sodium Pyruvate and 5% FBS. Primary epidermal melanocytes were grown in Dermal Cell Basal Medium (ATCC, Cat# PCS-200-030) supplemented with Adult Melanocyte Growth Kit (ATCC, Cat# PCS-200-042). We added penicillin (50 U/ml) and streptomycin (50 lg/ml) to all growth media.

Small molecule inhibitors, including a library of 276 epigenetic-modifying compounds, chemicals used in the follow-up cell-based assays (Givinostat, CUDC-907, JIB-04, AZ6102, I-BET-762,

OTX015 and SP2509), as well as vemurafenib and trametinib were all purchased from Selleck Chemicals. SP2577 was purchased from MedChem Express. The complete list of compounds used in this study, their catalog numbers and purity, as evaluated by HPLC and MS analysis, are presented in Supplementary Table 1. Compounds used for cell-based studies were dissolved in the appropriate vehicle (either DMSO or water) at a stock concentration of 10 mM. The vehicle for SP2577 used for *in vivo* studies is described below.

The following primary monoclonal antibodies (mAb, clone name) and polyclonal antibodies (pAb) with specified animal sources, catalog numbers and dilution ratios, were used in immunofluorescence staining assays: MITF (mouse mAb, clone D5, Abcam, Cat# ab3201, 1:800), p-ERK$^{T202/Y204}$ (rabbit mAb, clone D13.14.4E, Cell Signaling Technology, Cat# 4370, 1:800), Ki-67 (mouse mAb, clone 8D5, Cell Signaling Technology, Cat#9449, 1:1200), AXL (goat pAb, R&D Systems, Cat# AF154, 1:400), p-Rb$^{S807/811}$ (goat pAb, Santa Cruz Biotechnology, Cat# sc-16670, 1:400), NGFR (rabbit mAb, clone D4B3, Cell Signaling Technology, Cat# 8238, 1:1600), p-S6$^{S235/S236}$ (rabbit mAb, clone D57.2.2E, Cell Signaling Technology, Cat# 4851, 1:400), SOX10 (mouse mAb, clone SOX10/991, Abcam, Cat# ab212843, 1:1200), p-H2A.X^{S139} (rabbit mAb, clone EP854(2)Y, Abcam, Cat# ab195188, 1:700), KDM1A (rabbit mAb, clone C69G12, Cell Signaling Technology, Cat# 2184, 1:400), KDM4A (rabbit mAb, clone C37E5, Cell Signaling Technology, Cat# 5328, 1:200), KDM4B (rabbit mAb, clone D7E6, Cell Signaling Technology, Cat# 8639, 1:800), KDM5A (rabbit mAb, clone EPR18651, Abcam, Cat# ab194286, 1:200), and KDM5B (rabbit mAb, clone EPR12704, Abcam, Cat# ab181089, 1:400). The following secondary antibodies with specified sources and catalog numbers were used at a 1:2000 dilution: anti-rabbit Alexa Fluor 488 (Thermo Fisher, Cat# A21206), anti-mouse Alexa Fluor 647 (Thermo Fisher, Cat# A31571), anti-goat Alexa Fluor 568 (Thermo Fisher, Cat# A11057),

anti-mouse Alexa Fluor 568 (Thermo Fisher, Cat# A10037), and anti-rabbit Alexa Fluor 647 (Thermo Fisher, Cat# A31573).

Immunofluorescence staining, quantitation and analysis

Cells in 96-well plates were fixed in either 4% paraformaldehyde (PFA) for 20 min at room temperature or 100% ice-cold methanol for 15 min at -20°C. Cells were then washed with PBS, permeabilized in methanol (in cases where they were fixed with 4% PFA) for 10 min at -20°C, rewashed with PBS, and blocked using Odyssey blocking buffer (LI-COR Biosciences) for 1 h at room temperature. Cells were incubated overnight (~16 h) at 4°C with primary antibodies in Odyssey blocking buffer. The following day, cells were washed three times with PBS supplemented with 0.1% Tween-20 (Sigma-Aldrich) (PBS-T) and incubated for 1 h at room temperature with the secondary rabbit, goat, or mouse antibodies. Cells were then washed once with PBS-T, once in PBS, and then incubated with Hoechst 33342 (Thermo Fisher, Cat# H3570, 1:20000) for 20 min at room temperature. Cells were washed twice with PBS and imaged with a 10x objective using the ImageXpress Micro Confocal High-Content Imaging System (Molecular Devices). A total of 9 sites were imaged per well. Background subtraction was performed with ImageJ, whereas image segmentation and signal intensity quantification were performed with CellProfiler [46]. Population-average and single-cell data were analyzed using MATLAB 2019b. By generating histograms of single-cell data across a variety of conditions for each protein (X), including positive and negative controls, we identified an appropriate binary gate, based on which the percentage of X^{High} versus X^{Low} cells in each condition was quantified.

Single-cell analysis and dimensionality reduction

To visualize baseline and treatment-induced single-cell heterogeneities in a two-dimensional space, we

used a population of 6069 cells assembled following random selection of 60 individual cells (or fewer in the case of the highly drug-sensitive C32 cell line, for which <60 cells survived following treatments with the combination of vemurafenib and trametinib) from each of the 102 tested conditions, covering the entire panel of 17 cell lines, 3 drugs (DMSO, vemurafenib alone, and vemurafenib plus trametinib) and 2 timepoints. Log-transformed single-cell data for multiplexed measurements of differentiation state markers, MITF, NGFR and AXL, and for multiplexed measurements of MAPK signaling, p-ERK$^{T202/Y204}$, p-S6$^{S235/S236}$ and Ki-67, were processed by z-scoring (for each protein measurement) across all 6069 cells, followed by principal component analysis (PCA) using the MATLAB built-in function 'pca'. 80% of the variance in the differentiation state single-cell data and 92.5% of the variance in MAPK single-cell data were captured by the first two principal components (PCs). We thus performed *t*-distributed stochastic neighbor embedding (t-SNE) analysis on the scores from the first two PCs of each of the single-cell datasets by applying the built-in 'tsne' function in MATLAB 2019b. We used the 'barneshut' algorithm, learning rate of 1000 for the optimization process, a maximum number of optimization iterations of 2000, perplexity of 480, and exaggeration factor of 4.

Measurements of growth rate, drug sensitivity and combination effectiveness

Growth rate inhibition assays were performed in 96-well clear bottom black plates (Corning, Cat# 3904). Cells were counted using a TC20 automated cell counter (Bio-Rad Laboratories) and seeded in 200 µl of full growth media at a density of 1,200-5,000 cells per well, depending on the baseline proliferation rate of each cell line. Using a D300e Digital Dispenser, cells were treated the next day with small molecule compounds at reported doses or vehicle (DMSO). Measurements of live cell count across multiple timepoints were then used to calculate the net growth rate for each treatment condition. To measure the number of surviving cells at each timepoint, cells were fixed in 4% paraformaldehyde

for 20 min at room temperature. Cells were washed twice with PBS and incubated with Hoechst 33342 (Thermo Fisher, Cat# H3570, 1:20000) for 20 min at room temperature. Cells were washed again with PBS and imaged with a 10x objective using an ImageXpress Micro Confocal High-Content Imaging System (Molecular Devices). A total of 9 sites were imaged per well. Nuclear segmentation and cell counting was performed using CellProfiler [46].

The net growth rate for cells treated with individual compounds (including MAPK inhibitors or epigenetic inhibitors), or their combination, or vehicle, was calculated from time-dependent changes in live cell counts according to the following equation:

$$\mu = \frac{ln\left(\frac{N_{t2}}{N_{t1}}\right)}{t_2 - t_1}$$

where N_{t1} and N_{t2} represent the number of cells measured at timepoints $t = t_1$ and $t = t_2$, respectively, and μ describes the net growth rate of cells during the time period between t_1 and t_2. Average net growth rates for each treatment condition were calculated as the mean of growth rates measured across multiple consecutive timepoints. To compare drug sensitivity among cell lines while correcting for differences in their baseline proliferation rates, drug-induced normalized growth rates (a.k.a. DIP rates [36]) were computed as follows:

$$Normalized\ growth\ rate\ (DIP) = \frac{\mu_{drug}}{\mu_{DMSO}}$$

As shown above, normalized growth rate for cells treated with a specific drug is calculated by normalizing the average net growth rate measured for drug-treated cells (μ_{drug}) to that measured for vehicle (DMSO)-treated cells (μ_{DMSO}). Normalized growth rates < 0 indicate a net cell loss (i.e. cytotoxicity), a value of 0 represents no change in viable cell number (i.e. cytostasis), a value > 0 indicates a net cell gain (i.e. population growth), and a value of 1 represents cell growth at the same rate as in vehicle-treated (control) cells.

To quantify the benefit resulting from combining drugs, e.g. an epigenetic inhibitor (A) with a MAPK inhibitor (B), in comparison with using either of drugs alone, we computed drug combination index (CI) values as follows:

$$CI = \frac{\mu_{A+B} - \min(\mu_A, \mu_B)}{\mu_{DMSO}}$$

where μ_{DMSO} represents growth rate for DMSO-treated cells, μ_{A+B} represents the effect of combination treatment (i.e. growth rate in the presence of epigenetic inhibitor plus MAPK inhibitor), and $\min(\mu_A, \mu_B)$ represents the effect of the most efficacious individual treatment (i.e. the smaller of the growth rates between the epigenetic inhibitor and MAPK inhibitor treatments). This definition is consistent with the framework proposed by Gaddum [37] (a.k.a. the Highest Single Agent model), where any combined effect stronger than a single drug (CI < 0) is called synergism, any effect weaker than a single drug (CI > 0) is called antagonism, and a combined effect exactly equal to the strongest single drug (CI = 0) shows the dominance of that drug relative to the other one. In contrast to Loewe Additivity [47] or Bliss Independence [48], the Highest Single Agent model can be applied to unbounded drug effects such as the normalized growth rates measured in this study [49]. Using this framework, we identify any interaction that causes the combination of two drugs to be more effective in reducing the net growth rate (via either inhibition of cell division or induction of cell death) than either of the constituent drugs without drawing a distinction between synergism, additivity or even sub-additive effects.

Epigenetic compound screen

COLO858 and MMACSF cells were counted using a TC20 automated cell counter (Bio-Rad Laboratories) and seeded in 96-well clear bottom black plates at 2000 and 3000 cells per well (excluding 36 wells at the edges), respectively. Using the HP D300e Digital Dispenser, cells were treated the next day with either vehicle (DMSO or water) or two different doses (0.2 μM and 1 μM) of each of the 276

compounds in an epigenetic compound library. After 24 h, cells were either fixed or treated with vemurafenib alone (at 100 nM), or vemurafenib (at 100 nM) plus trametinib (at 10 nM), or vehicle (DMSO). Cells were then grown for a further 72 h or 120 h prior to fixation. All experimental conditions with an epigenetic compound treatment (at each dose and timepoint) were tested in two replicates. Experimental conditions that did not include an epigenetic compound treatment (i.e. treatments with only vehicle, vemurafenib, or vemurafenib in combination with trametinib) were repeated in all 96-well plates during the entire period of compound screening, creating a total of 276 replicates that were used to evaluate plate-to-plate and day-to-day experimental robustness. To differentiate the impact of epigenetic compounds on each cell line at different states of MAPK signaling, the growth rates for cells treated with each dose of an epigenetic compound were compared with growth rates for cells treated without any epigenetic compound, following 72 h and 120 h of exposure to each of the MAPK inhibitor treatment conditions (i.e., DMSO, vemurafenib, and vemurafenib plus trametinib). Significant epigenetic compounds were defined as those that led to a statistically significant decrease in normalized growth rate (with an effect size of at least 0.5 day^{-1}) in at least one of the tested conditions (i.e. cell lines, timepoints, or MAPK inhibitor conditions). Statistical significance was evaluated as $P < 0.05$ based on two-sample *t*-test following correction for multiple comparisons using the Dunn-Sidak method. To analyze the baseline state and treatment-induced changes in the single-cell behavior of each cell line, we used the t-SNE map overlaid with the projection of z-scored single-cell measurements (color coded between blue and red) for that cell line while showing data for other cell lines in gray.

Hierarchical clustering

To infer potential variations in the mechanisms of action of the selected group of 58 epigenetic compounds, treatment-induced changes in growth rate, p-$ERK^{T202/Y204}$, p-$Rb^{S807/811}$, and MITF across

different cell lines and MAPK inhibitor conditions were integrated into a matrix for unsupervised clustering. Growth rates for epigenetic inhibitor conditions were averaged across three timepoints and two doses of the inhibitor and their differences relative to the time-averaged growth rate in the absence of any epigenetic compound were used for each MAPK inhibitor treatment condition (i.e., DMSO, vemurafenib, and vemurafenib plus trametinib). For p-ERK$^{T202/Y204}$, p-Rb$^{S807/811}$, and MITF, log-transformed signal intensities (from quantitative immunofluorescence microscopy) were averaged across three timepoints and two doses of the inhibitor and their differences relative to the corresponding MAPK inhibitor condition in the absence of any epigenetic compound were used. Unsupervised hierarchical clustering of the integrated data was then carried out using MATLAB 2018b with the Correlation distance metric and the Complete (farthest distance) algorithm for computing the distance between clusters.

Statistical analysis of drug response data

All data with error bars were presented as mean values ± standard deviation (s.d.) using indicated numbers of replicates. The significance of pairwise correlations among drug response data were evaluated based on *P* values associated with the corresponding Pearson's correlation coefficients (*r*). The statistical significance of the effects of epigenetic compounds (in the first stage of screen) was evaluated based on $P < 0.05$ generated from two-sample *t*-test following correction for multiple comparisons using the Dunn-Sidak method. To identify the statistical significance of differences between mean or median of measurements within two different groups, *P* values from two-sample *t* test or from nonparametric Mann-Whitney U-test were used, respectively. Statistical significance of the difference in % change in tumor size in mouse experiments was determined by two-way analysis of variance (ANOVA). Statistical analyses were performed using MATLAB 2019b software.

Partial least square regression (PLSR) analysis

We used partial least square regression (PLSR) analysis [18,39,50] to generate models that linked epigenetic treatment-induced changes in normalized growth rates to baseline and treatment-induced changes in signaling and phenotypic data. By combining data for each epigenetic inhibitor across eight cell lines, we generated one model to predict responses to each epigenetic inhibitor, when used either individually or in combination with BRAF/MEK inhibitors. "Response" variables for each model were defined as normalized growth rates (averaged across 3-5 days of treatment) in the absence or presence of that compound (together with either DMSO, vemurafenib alone, or vemurafenib in combination with trametinib) across the eight cell lines. "Input" vectors were constructed by combining measurements of a total of 8 proteins (including signaling proteins, differentiation state and phenotypic markers) at the baseline (i.e. either DMSO, vemurafenib alone, or vemurafenib in combination with trametinib), following epigenetic inhibitor treatment (together with either DMSO, vemurafenib alone, or vemurafenib in combination with trametinib), and their changes induced by the epigenetic inhibitor which were computed by taking the ratio of the two sets of measurements. All protein measurements were performed by quantitative immunofluorescence microscopy, log-transformed and averaged cross three timepoints (including 24 after epigenetic inhibitor or DMSO treatment, followed by 72 h and 120 h of MAPK inhibitor or DMSO treatment). The data were then z-scored across all conditions and cell lines prior to the application of PLSR analysis using the built-in MATLAB function 'plsregress'.

To evaluate the predictability of the linear relationship between the input and output variables in each model, we used leave-one-out cross validation. The goodness of fit for each model was calculated using R^2. Prediction accuracy was evaluated by Q^2 and the *P* values generated from pairwise Pearson's correlations between the measured and predicted responses following cross-validation. For the

assessment of relative variable importance in each PLSR model, the information content of each variable was assessed by its variable importance in the projection (VIP) [40].

Gene knockdown by siRNA

For siRNA-mediated knockdown experiments, WM115, WM902B and A2058 cells were seeded in 200 µl of antibiotic-free growth media in 96-well clear bottom black plates at seeding densities of 3500, 4000, and 1700 cells per well, respectively. After 24 hours, cells were transfected using the DharmaFECT 1 transfection reagent (GE Dharmacon T-2001-01) with Dharmacon's ON-TARGETplus Human SMARTpool siRNAs for KDM4A (L-004292-00-0005), KDM4B (L-004290-00-0005), KDM5A (L-003297-02-0005), KDM5B (L-009899-00-0005), or non-targeting control (D-001810-10-05) at 25 nM each. To evaluate the effect of BRAF/MEK inhibition in cells in which either of the proteins were knocked down, WM115 and WM902B cells were further treated with vemurafenib (at 100 nM) plus trametinib (at 10nM) or DMSO 48 h following siRNA addition. After another 48 h, cells were fixed and analyzed using quantitative immunofluorescence microscopy.

Gene knockout by CRISPR-Cas9

A2058 cells were seeded in a 24-well plate at a seeding density of 30,000 cells per well for 24 hours. The next day, cells were treated at MOI of 0.3 with the pre-designed Edit-R lentiviral Cas9 nuclease (Dharmacon, Cat# VCAS10124). Polybrene (at 8 µg/ml) was added to enhance efficiency of the viral infection. Following an incubation period of 72 h with the lentivirus, Cas9-lentiviral-treated cells were selected with blasticidin over a period of 1.5 weeks. Surviving A2058 Cas9-positive cells were subsequently infected with either non-targeting control (Dharmacon, Cat# VSGC10216) or KDM1A lentiviral sgRNAs (Dharmacon, Cat# VSGH10142-246522030, VSGH10142-246999191, and

VSGH10142-246522028). The efficiency of KDM1A knockout and the consequential changes in cell viability were measured via immunostaining for the KDM1A protein at 96 h, followed by quantitative immunofluorescence microscopy.

In vivo xenograft assays

All mouse experiments were carried out in accordance with procedures approved by the Institutional Animal Care and Use Committee (IACUC) at the University of Michigan. Athymic, 5-6 weeks old female nude (NU/J) mice were purchased from The Jackson Laboratory. Mice were maintained and housed under standard animal housing protocol at the University of Michigan Unit for Laboratory Animal Care (ULAM). For xenograft tumor injections, mice were first anesthetized using 3% vaporized isoflurane. 2.5×10^6 cells from either of the melanoma cell lines A375 or WM2664 suspended in 200 µl of growth factor-reduced Matrigel (Thermo Fisher, CB-40230C) in PBS (1:1) were injected subcutaneously in the right flank of each mouse. Tumor xenografts were monitored three times a week with digital calipers. Once the tumors were palpable and the mean volume across all tumors reached a volume of approximately 170 mm^3, the mice were randomly allocated to two treatment groups of 5 mice per group. SP2577 (at a daily dose of 80 mg/kg) or vehicle (20% DMSO, 20% Cremophor EL, plus 60% sterile water) was then administered to each mouse via I.P. injection of a solution of 200 µl. Mouse body weight, tumor volume, and general health were monitored three times a week for 12 days. At the endpoint of the study, mice were euthanized by CO_2 asphyxiation and bilateral pneumothorax.

Data availability

Source data for all high-throughput experiments, including growth rate inhibition assays, epigenetic compound screening, single-cell profiling of MAPK signaling and differentiation state in melanoma

cells, as well as profiling of signaling and phenotypic responses to epigenetic inhibitors are presented in Supplementary Datasets 1-7.

Code availability

Custom analysis MATLAB scripts are available upon request.

Acknowledgments

We thank Meenhard Herlyn for excellent advice. We also thank Noah Brown, LaJuanda Carter and members of the Fallahi-Sichani laboratory for help and discussion. This work was supported by the University of Michigan Medical School and awards from the Elsa Pardee Foundation and V Foundation for Cancer Research V2017-011, Department of Defense PRCRP Career Development Award W81XWH1810427, NIH grants R00-CA194163 and R35-GM133404 (to MFS), P30-CA046592 (University of Michigan Rogel Cancer Center), NCI Training Grant award T32-CA009676 (to MK), the Welch Foundation I-1878 and CPRIT RP160493 (to EDM) and NCI SPORE grant P50-CA70907.

Author Contributions

M.K. designed and performed the experiments, analyzed the experimental data, performed analyses, and wrote the manuscript. M.M. designed and performed the experiments. E.D.M. synthesized reagents for the experiments. M.F.-S. designed the experiments, performed analyses and wrote the manuscript.

Statement of Competing Interests

The authors declare no competing financial interests.

Figure Legends

Figure 1. Single-cell analysis uncovers heterogeneities in melanoma differentiation, proliferation and MAPK signaling states across a wide range of BRAF/MEK inhibitor sensitivity. (a,b) Single-cell protein levels of three melanoma differentiation state markers, including MITF (representing the melanocytic phenotype), NGFR (representing the neural crest-like phenotype), and AXL (representing the undifferentiated phenotype), measured by multiplexed immunofluorescence microscopy and overlaid on t-SNE plots. A total population of 6069 randomly selected cells, including approximately sixty cells from each of the 16 $BRAF^{V600E/D}$ melanoma cell lines or primary melanocytes following exposure to either vehicle (DMSO), BRAF inhibitor (vemurafenib at 100 nM), or the combination of BRAF and MEK inhibitors (vemurafenib at 100 nM and trametinib at 10 nM) for 3 and 5 days were included in the analysis. For comparison purposes, we also analyzed an $NRAS^{Q61K}$-mutated isogenic variant of the A375 cell line (A375-$BRAF^{V600E}$/$NRAS^{Q61K}$), representing a common mechanism of acquired (late) resistance detected in ~20% of melanomas following progression on BRAF/MEK-targeted therapies. Cells for each experimental condition were randomly selected from the pool of two replicates. Single-cell t-SNE maps for all cell lines combined **(a)** and projections of heterogeneity within each individual cell line **(b)** are shown. See also Supplementary Dataset 1. **(c,d)** Single-cell protein levels of MAPK signaling and proliferation state markers, including p-$ERK^{T202/Y204}$, p-$S6^{S235/S236}$, and Ki67, measured by multiplexed immunofluorescence microscopy and overlaid on t-SNE plots. Approximately sixty cells from each of the 16 $BRAF^{V600E/D}$ melanoma cell lines or primary melanocytes following exposure to either vehicle (DMSO), BRAF inhibitor (vemurafenib at 100 nM), or the combination of BRAF and MEK inhibitors (vemurafenib at 100 nM and trametinib at 10 nM) for 3 and 5 days were included in the analysis. Single-cell t-SNE maps for all cell lines combined **(c)** and projections of heterogeneity within each individual cell line **(d)** are shown. See also Supplementary Dataset 2. **(e)** Average net growth rates

calculated from measurements of live cell count (across at least two replicates) at three timepoints (including 0, 3, and 5 days) following exposure to DMSO, vemurafenib (at 100 nM) or vemurafenib (at 100 nM) plus trametinib (at 10 nM). See also Supplementary Dataset 3. **(f)** Drug-induced normalized growth rates (a.k.a. DIP rates) calculated by dividing the average net growth rate for drug-treated cells to that for DMSO-treated cells in each cell line. Normalized growth rates < 0 indicate a net cell loss (i.e. drug-induced cytotoxicity), a value of 0 represent no change in viable cell number (i.e. cytostasis), a value > 0 indicates a net cell gain (i.e. population growth in the presence of drug), and a value of 1 represents no drug effect as cells grow at the same rate as in the DMSO condition. **(g)** Pairwise Pearson correlation analysis between the fraction of p-ERK^{Low}/p-S6^{Low}/Ki-67^{Low} cells (referred to as fully inhibited cells) and drug-induced normalized growth rate (top left), the fraction of undifferentiated (NGFR^{Low}/AXL^{High}) cells (top right), the fraction of neural crest-like (NGFR^{High}/AXL^{Low}) cells (bottom left), and the fraction of melanocytic (MITF^{High}) cells (bottom right) across 16 melanoma cell lines treated with BRAF/MEK inhibitors for 3 and 5 days.

Figure 2. A chemical screen identifies epigenetic modulators of phenotypic heterogeneity. (a) t-SNE maps comparing single-cell heterogeneity in differentiation state (MITF, NGFR and AXL) and MAPK signaling (p-ERK$^{T202/Y204}$, p-S6$^{S235/S236}$ and Ki67) within two BRAF^{V600E} melanoma cell lines, MMACSF and COLO858, following exposure to vehicle (DMSO), vemurafenib (at 100 nM), alone or in combination with trametinib (at 10 nM), for 72 and 120 h. **(b)** Log_2-normalized, time-dependent changes in live cell count following exposure of COLO858 and MMACSF cells to either DMSO, vemurafenib (at 100 nM), or vemurafenib (at 100 nM) plus trametinib (at 10 nM), for a period of 120 h. Cells were pretreated for 24 h with either DMSO (top panels) or two different doses (0.2 and 1 μM) of each of the 276 epigenetic-modifying compounds (bottom panels). Data represent mean values ± s.d.

calculated across replicates. See also Supplementary Dataset 4. **(c)** A schematic representation of the overall procedure of data collection, processing (normalization), integration and hierarchical clustering using measurements of cellular grow rate, MITF, p-Rb$^{S807/811}$, and p-ERK$^{T202/Y204}$ at indicated treatment conditions and timepoints in MMACSF and COLO858 cells. Unsupervised clustering analysis was performed on data collected for 58 epigenetic compounds that led to a statistically significant decrease in normalized growth rate (when used either as a single agent, or in combination with BRAF/MEK inhibitors) in either or both of cell lines. Prior to clustering, data collected for cells treated with each epigenetic compound and MAPK inhibitor condition (i.e., DMSO, vemurafenib, or vemurafenib plus trametinib) were normalized to cells treated without any epigenetic compound and the same MAPK inhibitor condition. Groups of compounds with similar nominal epigenetic targets are listed on the right side. See also Supplementary Dataset 5.

Figure 3. Patterns of melanoma responsiveness to mechanistically distinct epigenetic inhibitors, when used individually or in combination with BRAF/MEK inhibitors. (a) Epigenetic compounds (and their nominal protein targets) used in the second stage of epigenetic compound screen. **(b)** Measurements of normalized growth rate (averaged across at least 2 replicates) induced by each epigenetic inhibitor, when used either as a single agent (left), in combination with vemurafenib (middle), or in combination with vemurafenib plus trametinib (right), across eight different BRAF-mutant melanoma cell lines and non-transformed primary melanocytes. Treatment doses for different compounds are as follows: Givinostat (200 nM), CUDC-907 (20 nM), JIB-04 (200 nM), AZ6102 (1 μM), I-BET-762 (1 μM), OTX015 (0.2 μM), SP2509 (1 μM). Cells were pre-treated with the indicated epigenetic compounds for 24 h and then treated for a period of 3-5 days with either DMSO, vemurafenib (at 100 nM) or the combination of vemurafenib (at 100 nM) and trametinib (at 10 nM). See also

Supplementary Dataset 6. **(c)** Drug combination index (CI) values computed based on the Highest Single Agent (HSA) model across diverse epigenetic inhibitor treatments and cell lines. CI represents the difference between the effect of combination treatment (i.e. normalized growth rate in the presence of epigenetic inhibitor plus the indicated MAPK inhibitor treatment) and that of the most efficacious individual treatment (i.e. the smaller of the normalized growth rates between epigenetic inhibitor and the indicated MAPK inhibitor treatment). As defined by the HSA model, any combined effect stronger than a single drug (CI < 0) is called synergism, any effect weaker than a single drug (CI > 0) is called antagonism, and a combined effect exactly equal to the strongest single drug (CI = 0) shows the dominance of one drug relative to the other one. **(d)** Pairwise Pearson correlations between the effects (i.e. normalized growth rates) of mechanistically distinct epigenetic inhibitors (used individually or in combination with vemurafenib or vemurafenib plus trametinib) evaluated across eight BRAF-mutant melanoma cell lines.

Figure 4. Correlated patterns of vulnerability to pharmacological inhibition of KDM1A, Jmj-KDMs and BET proteins across 16 BRAF-mutant melanoma cell lines. (a) Pairwise Pearson correlations between the effects (i.e. normalized growth rates) of KDM1A inhibitor SP2509 (at 1 μM), Jmj-KDM inhibitor JIB-04 (at 200 nM), and BET inhibitors OTX015 (at 200 nM) and I-BET762 (at 1 μM), used individually or in combination with vemurafenib (at 100 nM) plus trametinib (at 10 nM) and evaluated across sixteen BRAF-mutant melanoma cell lines. See also Supplementary Dataset 6. **(b)** Log_2-normalized, time-dependent changes in live cell count following exposure of seven selected melanoma cell lines and non-transformed primary melanocytes to different drugs at indicated doses for a period of 5 days. MMACSF, WM115 and WM902B cell lines represent cell lines that exhibit high sensitivity to the combination of JIB-04 or BET inhibitors with BRAF/MEK inhibitors, while being

resistant to SP2509. A2058, A375 and A375(NRAS^{Q61K}) represent cell lines that are highly sensitive to SP2509. HS294T cells show partial sensitivity to either of the compounds. Data represent mean values ± s.d. calculated from two replicates per treatment condition. **(c)** Measurements of normalized growth rate (left) and drug combination index values computed based on the HSA model (right) across diverse epigenetic inhibitor treatments and sixteen BRAF-mutant melanoma cell lines. Experimental conditions and the analysis approach are the same as Fig. 3. **(d)** Log_2-normalized, time-dependent changes in live cell count following exposure of three selected melanoma cell lines to different drugs at indicated doses for a period of 20 days. Data represent mean values ± s.d. calculated from four replicates per treatment condition.

Figure 5. **Multivariate computational modeling identifies differentiation state-specific predictors of epigenetic inhibitor efficacy. (a)** Baseline and treatment-induced changes in protein measurements of melanoma differentiation state markers (NGFR, AXL, MITF, SOX10), MAPK signaling protein modifications (ERK$^{T202/Y204}$, p-S6$^{S235/S236}$), a proliferation marker (Ki-67), and a DNA damage response marker (p-H2A.X^{S139}), across eight melanoma cell lines following treatment with the indicated epigenetic compounds, either individually or in combination with vemurafenib, or vemurafenib plus trametinib. Treatment doses for different compounds are as follows: Givinostat (200 nM), CUDC-907 (20 nM), JIB-04 (200 nM), AZ6102 (1 μM), I-BET-762 (1 μM), OTX015 (0.2 μM), SP2509 (1 μM). Cells were pre-treated with the indicated epigenetic compounds for 24 h and then treated for a period of 3-5 days with either DMSO, vemurafenib (at 100 nM) or the combination of vemurafenib (at 100 nM) and trametinib (at 10 nM). Protein data shown for each condition represent mean values across three timepoints and two replicates and are then z-scored across all cell lines and treatment conditions. See also Supplementary Dataset 7. **(b)** Pairwise Pearson correlation between responses (normalized growth

rates) to SP2509 (left) or JIB-04 in combination with vemurafenib and trametinib (right), measured for each of the eight melanoma cell lines (x-axis) and corresponding responses predicted by partial least square regression (PLSR) modeling following leave-one-out cross validation (y-axis). **(c)** PLSR-derived variable importance in the projection (VIP) scores, highlighting combinations of protein measurements at the baseline (shown in red), following epigenetic inhibitor treatment (shown in blue), or the ratio of change induced by each epigenetic compound (shown in black), that are predictive of efficacy for SP2509 (left) and JIB-04 in combination with vemurafenib and trametinib (right). The sign of VIP score shows whether the change in variable correlated negatively or positively with the treatment-induced response. Only VIP scores of greater than 1 or smaller than -1 with a statistically significant Pearson correlation ($P < 0.05$) are highlighted. **(d)** Pairwise Pearson correlation analysis between the baseline fraction of undifferentiated (AXL^{High}) cells and measurements of normalized growth rate in response to SP2509 when used as a single agent (left), and between the baseline fraction of neural crest-like ($NGFR^{High}/AXL^{Low}$) cells and drug combination index for treatments with JIB-04, vemurafenib and trametinib (right), across sixteen BRAF-mutant melanoma cell lines.

Figure 6. KDM protein levels determine differentiation state-specific sensitivity to KDM inhibitors. (a) Pairwise Pearson correlation between drug combination index for JIB-04 plus vemurafenib and trametinib and protein levels of each of the JIB-04 targets, KDM4A, KDM4B, KDM5A and KDM5B, across nine melanoma cell lines. Protein level data are from the Cancer Cell Line Encyclopedia (CCLE) proteomics database and z-scored across the nine cell lines. **(b)** Pairwise Pearson correlation between variation in KDM4B protein levels and the difference in NGFR and AXL protein levels across thirteen melanoma cell lines. Protein level data are extracted from the Cancer Cell Line Encyclopedia (CCLE) proteomics database and z-scored across all of eighteen BRAF-mutant melanoma

cell lines present in the database. Five out of eighteen cell lines, for which at least one of the KDM4B, NGFR or AXL datapoints were missing, were excluded from this analysis. **(c)** Relative cell viability in WM115 cells (left), WM902B cells (middle) and A2058 cells (right) following treatment with indicated doses of the combination of vemurafenib and trametinib or vehicle (DMSO) in the presence of siRNAs targeting KDM4A, KDM4B, KDM5A, and KDM5B for 96 h. Viability data for each treatment condition were normalized to cells treated with DMSO and the non-targeting (control) siRNA. Data represent mean values ± s.d. calculated across 3 replicates. Statistical significance was determined by two-sided *t* test. **(d)** Relative cell viability in Cas9-positive A2058 cells following treatment with three different types of KDM1A lentiviral single guide RNA (sgRNA) for 96 h. Viability data were normalized to cells treated with non-targeting (control) sgRNA. Data represent mean values ± s.d. calculated across 4 replicates. Statistical significance was determined by two-sided *t* test. **(e)** Pairwise Pearson correlation between measurements of normalized growth rate for SP2509 and protein levels of KDM1A, ZNF217, and the sum of KDM1A and ZNF217, across nine melanoma cell lines. Protein level data are from the Cancer Cell Line Encyclopedia (CCLE) proteomics database and z-scored across the nine cell lines. **(f)** Pairwise Pearson correlation between variation in the sum of KDM1A and ZNF217 protein levels and AXL protein levels across sixteen melanoma cell lines. Protein level data are extracted from the Cancer Cell Line Encyclopedia (CCLE) proteomics database and z-scored across all of eighteen BRAF-mutant melanoma cell lines present in the database. Two out of eighteen cell lines, for which at least one of the KDM1A, ZNF217 or AXL datapoints were missing, were excluded from this analysis.

Supplementary Figure Legends

Supplementary Figure 1. Single-cell analysis uncovers heterogeneities in melanoma

differentiation, proliferation and MAPK signaling states across a wide range of BRAF/MEK inhibitor sensitivity. (a) Log_2-normalized changes in live cell count across three timepoints (including 0, 3, and 5 days) following exposure of 16 $BRAF^{V600E/D}$ melanoma cell lines and primary melanocytes to DMSO, vemurafenib (at 100 nM) or vemurafenib (at 100 nM) plus trametinib (at 10 nM). Data represent mean values ± s.d. calculated from two replicates per treatment condition. **(b)** Pairwise Pearson correlation analysis between diverse differentiation states, MAPK signaling states, and normalized growth rates cross 16 melanoma cell lines treated with BRAF inhibitor (vemurafenib at 100 nM) or the combination of BRAF and MEK inhibitors (vemurafenib at 100 nM and trametinib at 10 nM) for 3-5 days.

Supplementary Figure 2. Changes in MMACSF cellular growth rate induced by significant epigenetic treatments. Log_2-normalized, time-dependent changes in live cell count following exposure of MMACSF cells (pretreated for 24 h with either DMSO or two different doses of 58 significant epigenetic compounds) to either DMSO, vemurafenib (at 100 nM), or vemurafenib (at 100 nM) plus trametinib (at 10 nM), for a period of 3-5 days. Individual compounds and their nominal epigenetic targets are indicated. Data represent mean values ± s.d. calculated from two replicates per treatment condition.

Supplementary Figure 3. Changes in COLO858 cellular growth rate induced by significant epigenetic treatments. Log_2-normalized, time-dependent changes in live cell count following exposure of COLO858 cells (pretreated for 24 h with either DMSO or two different doses of 58 significant epigenetic compounds) to either DMSO, vemurafenib (at 100 nM), or vemurafenib (at 100 nM) plus trametinib (at 10 nM), for a period of 3-5 days. Individual compounds and their nominal epigenetic

targets are indicated. Data represent mean values ± s.d. calculated from two replicates per treatment condition.

Supplementary Figure 4. Differential regulation of cellular states by mechanistically distinct epigenetic-modifying compounds. (a) Hierarchical clustering of normalized measurements of cellular grow rate, MITF, p-Rb$^{S807/811}$, and p-ERK$^{T202/Y204}$ at indicated treatment conditions and timepoints in MMACSF and COLO858 cells. Analysis was performed on data collected for 58 epigenetic compounds that led to a statistically significant decrease in normalized growth rate (when used either as a single agent, or in combination with BRAF/MEK inhibitors) in either or both of cell lines. Prior to clustering, data collected for cells treated with each epigenetic compound and MAPK inhibitor condition (i.e., DMSO, vemurafenib, or vemurafenib plus trametinib) were normalized to cells treated without any epigenetic compound and the same MAPK inhibitor condition. The list of epigenetic compounds and their nominal protein targets are shown on the right side. **(b)** Cell line-specific changes in growth rate induced by each class of epigenetic treatments. Growth rate data collected for cells treated with each epigenetic compound and MAPK inhibitor condition (i.e., DMSO, vemurafenib, and vemurafenib plus trametinib) were normalized to cells treated without any epigenetic compound and the same MAPK inhibitor condition.

Supplementary Figure 5. Epigenetic treatment-induced changes in growth rates of 8 melanoma cell lines and primary melanocytes. Log_2-normalized, time-dependent changes in live cell count following exposure of eight different melanoma cell lines and non-transformed primary melanocytes (pretreated for 24 h with either DMSO or two different doses of seven different epigenetic compounds) to either DMSO, vemurafenib (at 100 nM), or vemurafenib (at 100 nM) plus trametinib (at 10 nM), for

a period of 3-5 days. Treatment doses for each compound are as follows: Givinostat (40 and 200 nM), CUDC-907 (20 and 100 nM), JIB-04 (40 and 200 nM), AZ6102 (0.2 and 1 μM), I-BET-762 (0.2 and 1 μM), OTX015 (0.2 and 1 μM), SP2509 (0.2 and 1 μM). Data represent mean values ± s.d. calculated from two replicates per treatment condition.

Supplementary Figure 6. Comparing treatment-induced changes in growth rates of melanoma cells following pharmacological inhibition of KDM1A, Jmj-KDMs and BET proteins. (a) Log_2-normalized, time-dependent changes in live cell count following exposure of melanoma cell lines and non-transformed primary melanocytes to different drugs at indicated doses for a period of 5 days. Data represent mean values ± s.d. calculated from two replicates per treatment condition. **(b)** Pairwise Pearson correlation between the effect (i.e. normalized growth rates) of KDM1A inhibitor SP2509 (at 0.2 μM) and its clinical formuylation, SP2577 (at 0.2 μM) across eight BRAF-mutant melanoma cell lines. (**c,d**) Mice bearing xenografts of WM2664 cells (**c**) and A375 cells (**d**) were treated as shown by the KDM1A inhibitor SP2577 or vehicle for a period of 12 days, to determine the effect on tumor growth. Data represent mean values ± s.e.m across 5 mice per group. Statistical significance was determined by two-way ANOVA.

Supplementary Figure 7. Multivariate computational modeling identifies differentiation state-specific predictors of epigenetic inhibitor efficacy. (a) Partial least square regression (PLSR) model calibration for the effect of each of the seven epigenetic inhibitors, used individually (left panels) or in combination with vemurafenib and trametinib (right panels), across eight BRAF-mutant melanoma cell lines. R^2 values (representing goodness of fit) and Q^2 values (representing prediction accuracy based on leave-one-out cross-validation) are shown for models built with increasing numbers of PLS components.

(b) Pairwise Pearson correlation between responses (normalized growth rates) to I-BET-762 in combination with vemurafenib and trametinib (left) or OTX015 in combination with vemurafenib and trametinib (right) measured for each of the eight melanoma cell lines (x-axis) and corresponding responses predicted by partial least square regression (PLSR) modeling following leave-one-out cross validation (y-axis). **(c)** PLSR-derived variable importance in the projection (VIP) scores highlighting combinations of protein measurements at the baseline (shown in red), following epigenetic inhibitor treatment (shown in blue), or the ratio of change induced by each epigenetic compound (shown in black), that are predictive of efficacy for I-BET-762 in combination with vemurafenib and trametinib (left) and for OTX015 in combination with vemurafenib and trametinib (right). The sign of VIP score shows whether the change in variable correlated negatively or positively with treatment-induced response. Only VIP scores of greater than 1 or smaller than -1 with a statistically significant Pearson correlation ($P < 0.05$) are highlighted. **(d)** Association of epigenetic compound efficacy with baseline melanoma differentiation state characterized at a single-cell level across sixteen BRAF-mutant cell lines. The significance of differences between normalized growth rate in response to SP2509 versus the baseline fraction of AXL^{High} cells (left panel), and differences between combination index values for JIB-04 or OTX015 plus vemurafenib and trametinib versus baseline fractions of $NGFR^{High}/AXL^{Low}$ cells, $NGFR^{High}$ cells, or $MITF^{Low}/AXL^{Low}$ cells was evaluated by *P* values based on nonparametric Mann-Whitney U-test. Sixteen cell lines were divided into two groups of eight based on whether the measured variable has a value above or below the median. Data for each group was then presented using box-and-whisker plots and median parameter values and interquartile ranges; bars extending to 1.5× the interquartile range are shown for each condition as a measure of variance. Parameter values for outlier cell lines are marked with asterisks.

Supplementary Figure 8. Effects of Jmj-KDM knockdown and KDM1A knockout on the corresponding protein expression levels at a single-cell level. (a) Single-cell protein levels of Jmj-KDM proteins KDM4A, KDM4B, KDM5A, and KDM5B, measured by immunofluorescence microscopy, in WM115 (top) and A2058 cells (bottom) following treatment with siRNAs targeting KDM4A, KDM4B, KDM5A, and KDM5B, or with non-targeting (control) siRNA for 96 h. **(b)** Single-cell protein levels of KDM1A, measured by immunofluorescence microscopy, in Cas9-positive A2058 cells following treatment with three different types of KDM1A lentiviral single guide RNA (sgRNA), or with non-targeting (control) sgRNA for 96 h.

Supplementary Tables

Supplementary Table 1. List of chemicals used in this study. Small molecule inhibitors, their nominal targets, their catalog numbers and purity are shown.

Supplementary Datasets

Supplementary Dataset 1. Single-cell protein levels of three melanoma differentiation state markers, including MITF, NGFR, and AXL, measured by multiplexed immunofluorescence microscopy across 16 $BRAF^{V600E/D}$ melanoma cell lines and primary melanocytes following exposure to either vehicle (DMSO), BRAF inhibitor (vemurafenib at 100 nM), or the combination of BRAF and MEK inhibitors (vemurafenib at 100 nM and trametinib at 10 nM) for 3 and 5 days. Data are associated with Fig. 1a, b.

Supplementary Dataset 2. Single-cell protein levels of MAPK signaling and proliferation state markers, including p-$ERK^{T202/Y204}$, p-$S6^{S235/S236}$, and Ki67, measured by multiplexed immunofluorescence microscopy across 16 $BRAF^{V600E/D}$ melanoma cell lines and primary melanocytes

following exposure to either vehicle (DMSO), BRAF inhibitor (vemurafenib at 100 nM), or the combination of BRAF and MEK inhibitors (vemurafenib at 100 nM and trametinib at 10 nM) for 3 and 5 days. Data are associated with Fig. 1c, d.

Supplementary Dataset 3. Measurements of live cell count for 16 $BRAF^{V600E/D}$ melanoma cell lines and primary melanocytes following exposure to either vehicle (DMSO), BRAF inhibitor (vemurafenib at 100 nM), or the combination of BRAF and MEK inhibitors (vemurafenib at 100 nM and trametinib at 10 nM) for 3 and 5 days. Data are associated with Fig. 1e, f.

Supplementary Dataset 4. Measurements of live cell count following exposure of COLO858 and MMACSF cells to either DMSO, vemurafenib (at 100 nM), or vemurafenib (at 100 nM) plus trametinib (at 10 nM) for a period of 72 or 120 h following pretreatment for 24 h with either DMSO or two different doses (0.2 and 1 μM) of each of the 276 epigenetic-modifying compounds. Data are associated with Fig. 2b.

Supplementary Dataset 5. Measurements of live cell count, MITF, p-$Rb^{S807/811}$, and p-$ERK^{T202/Y204}$ following exposure of COLO858 and MMACSF cells to either DMSO, vemurafenib (at 100 nM), or vemurafenib (at 100 nM) plus trametinib (at 10 nM) for a period of 72 or 120 h following pretreatment for 24 h with either DMSO or two different doses (0.2 and 1 μM) of each of the 58 significant epigenetic-modifying compounds. Data are associated with Fig. 2c.

Supplementary Dataset 6. Measurements of live cell count following exposure of 16 melanoma cell lines and non-transformed primary melanocytes to either DMSO, vemurafenib (at 100 nM), or

vemurafenib (at 100 nM) plus trametinib (at 10 nM) for a period of 72 or 120 h following pretreatment for 24 h with either DMSO or epigenetic compounds at indicated doses. Data are associated with Fig. 3 and 4.

Supplementary Dataset 7. Baseline and treatment-induced changes in protein measurements of melanoma differentiation state markers (NGFR, AXL, MITF, SOX10), MAPK signaling protein modifications ($ERK^{T202/Y204}$, $p\text{-}S6^{S235/S236}$), a proliferation marker (Ki-67), and a DNA damage response marker ($p\text{-}H2A.X^{S139}$), across eight melanoma cell lines following treatment with epigenetic compounds, either individually or in combination with vemurafenib, or vemurafenib plus trametinib. Cells were pre-treated with the indicated epigenetic compounds for 24 h and then treated for a period of 3-5 days with either DMSO, vemurafenib (at 100 nM) or the combination of vemurafenib (at 100 nM) and trametinib (at 10 nM). Data are associated with Fig. 5a.

References

1. Boumahdi, S. & de Sauvage, F. J. The great escape: tumour cell plasticity in resistance to targeted therapy. *Nat. Rev. Drug Discov.* (2019) doi:10.1038/s41573-019-0044-1.
2. Bai, X., Fisher, D. E. & Flaherty, K. T. Cell-state dynamics and therapeutic resistance in melanoma from the perspective of MITF and IFNγ pathways. *Nat. Rev. Clin. Oncol.* (2019) doi:10.1038/s41571-019-0204-6.
3. Hugo, W. *et al.* Non-genomic and Immune Evolution of Melanoma Acquiring MAPKi Resistance. *Cell* **162**, 1271–1285 (2015).
4. Sharma, S. V. *et al.* A chromatin-mediated reversible drug-tolerant state in cancer cell subpopulations. *Cell* **141**, 69–80 (2010).
5. Tong, K. *et al.* Degree of Tissue Differentiation Dictates Susceptibility to BRAF-Driven Colorectal Cancer. *Cell Rep.* **21**, 3833–3845 (2017).
6. Tsoi, J. *et al.* Multi-stage Differentiation Defines Melanoma Subtypes with Differential Vulnerability to Drug-Induced Iron-Dependent Oxidative Stress. *Cancer Cell* **33**, 890-904.e5 (2018).
7. Hinohara, K. *et al.* KDM5 Histone Demethylase Activity Links Cellular Transcriptomic Heterogeneity to Therapeutic Resistance. *Cancer Cell* **34**, 939-953.e9 (2018).
8. Hata, A. N. *et al.* Tumor cells can follow distinct evolutionary paths to become resistant to epidermal growth factor receptor inhibition. *Nat. Med.* **22**, 262–269 (2016).
9. Ku, S. Y. *et al.* Rb1 and Trp53 cooperate to suppress prostate cancer lineage plasticity, metastasis, and antiandrogen resistance. *Science* **355**, 78–83 (2017).
10. Fiziev, P. *et al.* Systematic Epigenomic Analysis Reveals Chromatin States Associated with Melanoma Progression. *Cell Rep.* **19**, 875–889 (2017).

11. Flaherty, K. T. *et al.* Combined BRAF and MEK inhibition in melanoma with BRAF V600 mutations. *N. Engl. J. Med.* **367**, 1694–1703 (2012).
12. Smith, M. P. *et al.* Inhibiting Drivers of Non-mutational Drug Tolerance Is a Salvage Strategy for Targeted Melanoma Therapy. *Cancer Cell* **29**, 270–284 (2016).
13. Fallahi-Sichani, M. *et al.* Adaptive resistance of melanoma cells to RAF inhibition via reversible induction of a slowly dividing de-differentiated state. *Mol. Syst. Biol.* **13**, 905 (2017).
14. Ravindran Menon, D. *et al.* A stress-induced early innate response causes multidrug tolerance in melanoma. *Oncogene* **34**, 4448–4459 (2015).
15. Su, Y. *et al.* Single-cell analysis resolves the cell state transition and signaling dynamics associated with melanoma drug-induced resistance. *Proc. Natl. Acad. Sci. U. S. A.* (2017).
16. Sun, C. *et al.* Reversible and adaptive resistance to BRAF(V600E) inhibition in melanoma. *Nature* **508**, 118–122 (2014).
17. Lito, P., Rosen, N. & Solit, D. B. Tumor adaptation and resistance to RAF inhibitors. *Nat. Med.* **19**, 1401–1409 (2013).
18. Fallahi-Sichani, M. *et al.* Systematic analysis of BRAF(V600E) melanomas reveals a role for JNK/c-Jun pathway in adaptive resistance to drug-induced apoptosis. *Mol. Syst. Biol.* **11**, 797 (2015).
19. Rambow, F. *et al.* Toward Minimal Residual Disease-Directed Therapy in Melanoma. *Cell* **174**, 843-855.e19 (2018).
20. Konieczkowski, D. J. *et al.* A melanoma cell state distinction influences sensitivity to MAPK pathway inhibitors. *Cancer Discov.* **4**, 816–827 (2014).

21. Roesch, A. *et al.* Overcoming intrinsic multidrug resistance in melanoma by blocking the mitochondrial respiratory chain of slow-cycling JARID1B(high) cells. *Cancer Cell* **23**, 811–825 (2013).

22. Liu, X. *et al.* KDM5B Promotes Drug Resistance by Regulating Melanoma-Propagating Cell Subpopulations. *Mol. Cancer Ther.* **18**, 706–717 (2019).

23. Shaffer, S. M. *et al.* Rare cell variability and drug-induced reprogramming as a mode of cancer drug resistance. *Nature* **546**, 431–435 (2017).

24. Johannessen, C. M. *et al.* A melanocyte lineage program confers resistance to MAP kinase pathway inhibition. *Nature* **504**, 138–142 (2013).

25. Tirosh, I. *et al.* Dissecting the multicellular ecosystem of metastatic melanoma by single-cell RNA-seq. *Science* **352**, 189–196 (2016).

26. Verfaillie, A. *et al.* Decoding the regulatory landscape of melanoma reveals TEADS as regulators of the invasive cell state. *Nat. Commun.* **6**, 6683 (2015).

27. Wellbrock, C. *et al.* Oncogenic BRAF regulates melanoma proliferation through the lineage specific factor MITF. *PloS One* **3**, e2734 (2008).

28. Lin, J. Y. & Fisher, D. E. Melanocyte biology and skin pigmentation. *Nature* **445**, 843–850 (2007).

29. Mica, Y., Lee, G., Chambers, S. M., Tomishima, M. J. & Studer, L. Modeling neural crest induction, melanocyte specification, and disease-related pigmentation defects in hESCs and patient-specific iPSCs. *Cell Rep.* **3**, 1140–1152 (2013).

30. Muller, J. *et al.* Low MITF/AXL ratio predicts early resistance to multiple targeted drugs in melanoma. *Nat. Commun.* **5**, 5712 (2014).

31. Emmons, M. F. *et al.* HDAC8 regulates a stress response pathway in melanoma to mediate escape from BRAF inhibitor therapy. *Cancer Res.* (2019) doi:10.1158/0008-5472.CAN-19-0040.

32. Maertens, O. *et al.* MAPK Pathway Suppression Unmasks Latent DNA Repair Defects and Confers a Chemical Synthetic Vulnerability in BRAF-, NRAS-, and NF1-Mutant Melanomas. *Cancer Discov.* **9**, 526–545 (2019).

33. Echevarría-Vargas, I. M. *et al.* Co-targeting BET and MEK as salvage therapy for MAPK and checkpoint inhibitor-resistant melanoma. *EMBO Mol. Med.* **10**, (2018).

34. Yu, Y. *et al.* Targeting the Senescence-Overriding Cooperative Activity of Structurally Unrelated H3K9 Demethylases in Melanoma. *Cancer Cell* **33**, 322-336.e8 (2018).

35. Corcoran, R. B. *et al.* TORC1 suppression predicts responsiveness to RAF and MEK inhibition in BRAF-mutant melanoma. *Sci. Transl. Med.* **5**, 196ra98 (2013).

36. Harris, L. A. *et al.* An unbiased metric of antiproliferative drug effect in vitro. *Nat. Methods* **13**, 497–500 (2016).

37. Gaddum, J. H. *Pharmacology*. (Oxford University Press, 1940).

38. Bayo, J. *et al.* Jumonji Inhibitors Overcome Radioresistance in Cancer through Changes in H3K4 Methylation at Double-Strand Breaks. *Cell Rep.* **25**, 1040-1050.e5 (2018).

39. Geladi, P. & Kowalski, B. R. Partial least-squares regression: a tutorial. *Anal. Chim. Acta* **185**, 1–17 (1986).

40. Wold, S. Exponentially weighted moving principal components analysis and projections to latent structures. *Chemom. Intell. Lab. Syst.* **23**, 149–161 (1994).

41. Wang, L. *et al.* A small molecule modulates Jumonji histone demethylase activity and selectively inhibits cancer growth. *Nat. Commun.* **4**, 2035 (2013).

42. Nusinow, D. P. *et al.* Quantitative Proteomics of the Cancer Cell Line Encyclopedia. *Cell* **180**, 387-402.e16 (2020).

43. Sehrawat, A. *et al.* LSD1 activates a lethal prostate cancer gene network independently of its demethylase function. *Proc. Natl. Acad. Sci. U. S. A.* **115**, E4179–E4188 (2018).

44. Haigis, K. M., Cichowski, K. & Elledge, S. J. Tissue-specificity in cancer: The rule, not the exception. *Science* **363**, 1150–1151 (2019).

45. Fontanals-Cirera, B. *et al.* Harnessing BET Inhibitor Sensitivity Reveals AMIGO2 as a Melanoma Survival Gene. *Mol. Cell* **68**, 731-744.e9 (2017).

46. McQuin, C. *et al.* CellProfiler 3.0: Next-generation image processing for biology. *PLoS Biol.* **16**, e2005970 (2018).

47. Loewe, S. & Muischnek, H. Effect of combinations: Mathematical basis of problem. *Arch. Exp. Pathol. Pharmacol* **114**, 313–326 (1926).

48. Bliss, C. I. The toxicity of poisons applied jointly. *Ann. Appl. Biol.* **26**, 585–615 (1939).

49. Meyer, C. T., Wooten, D. J., Lopez, C. F. & Quaranta, V. Charting the Fragmented Landscape of Drug Synergy. *Trends Pharmacol. Sci.* **41**, 266–280 (2020).

50. Janes, K. A. & Yaffe, M. B. Data-driven modelling of signal-transduction networks. *Nat. Rev. Cell Biol.* **7**, 820–828 (2006).

Figure 1

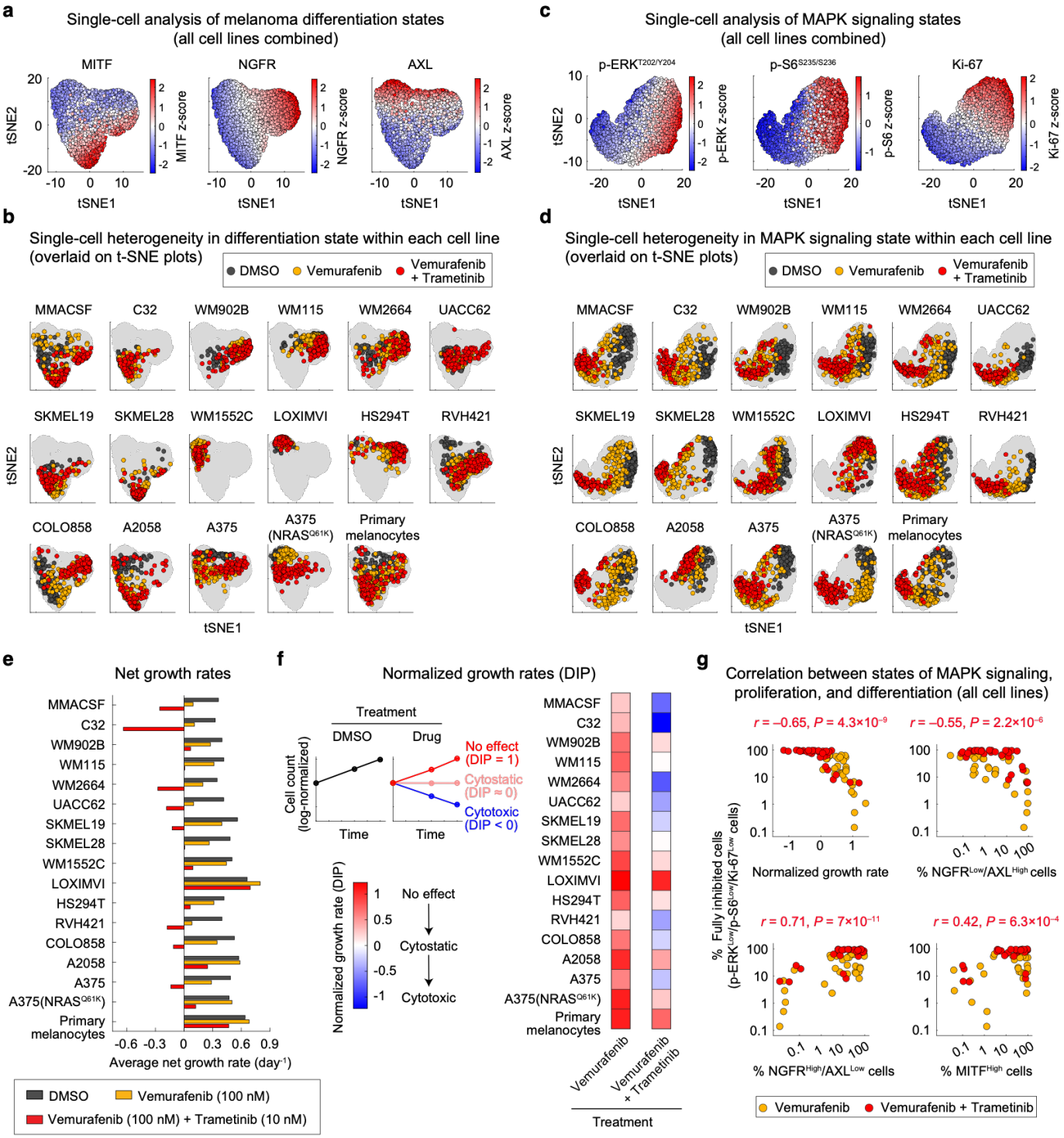
a
Single-cell analysis of melanoma differentiation states
(all cell lines combined)
MITF
NGFR
AXL
tSNE2
tSNE1
MITF z-score
NGFR z-score
AXL z-score
c
Single-cell analysis of MAPK signaling states
(all cell lines combined)
p-ERKT202/Y204
p-S6S235/S236
Ki-67
p-ERK z-score
p-S6 z-score
Ki-67 z-score
b
Single-cell heterogeneity in differentiation state within each cell line
(overlaid on t-SNE plots)
DMSO
Vemurafenib
Vemurafenib + Trametinib
MMACSF
C32
WM902B
WM115
WM2664
UACC62
SKMEL19
SKMEL28
WM1552C
LOXIMVI
HS294T
RVH421
COLO858
A2058
A375
A375 (NRASQ61K)
Primary melanocytes
d
Single-cell heterogeneity in MAPK signaling state within each cell line
(overlaid on t-SNE plots)
e
Net growth rates
Average net growth rate (day-1)
DMSO
Vemurafenib (100 nM)
Vemurafenib (100 nM) + Trametinib (10 nM)
f
Normalized growth rates (DIP)
Treatment
DMSO
Drug
Cell count (log-normalized)
Time
No effect (DIP = 1)
Cytostatic (DIP ≈ 0)
Cytotoxic (DIP < 0)
Normalized growth rate (DIP)
No effect
Cytostatic
Cytotoxic
Vemurafenib
Vemurafenib + Trametinib
g
Correlation between states of MAPK signaling, proliferation, and differentiation (all cell lines)
r = –0.65, P = 4.3×10–9
r = –0.55, P = 2.2×10–6
r = 0.71, P = 7×10–11
r = 0.42, P = 6.3×10–4
% Fully inhibited cells (p-ERKLow/p-S6Low/Ki-67Low cells)
Normalized growth rate
% NGFRLow/AXLHigh cells
% NGFRHigh/AXLLow cells
% MITFHigh cells
Vemurafenib
Vemurafenib + Trametinib

Figure 2

a

Single-cell heterogeneity in COLO858 versus MMACSF cells

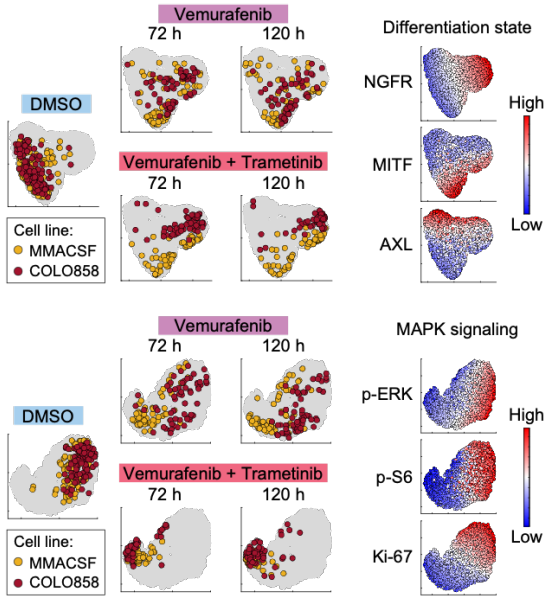

b

Responses to 276 epigenetic modifying compounds (1st stage screen)

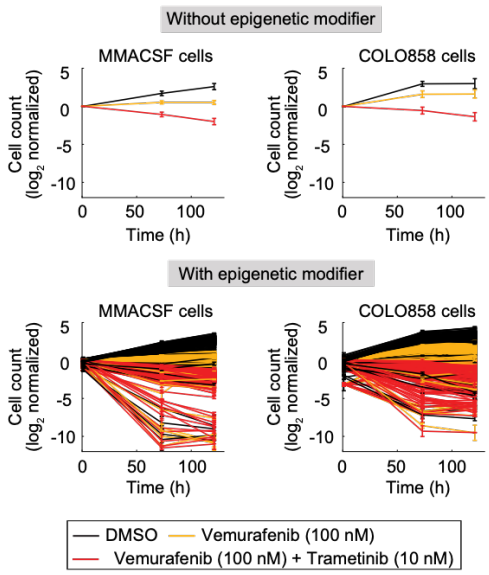

c

Processing of data across 58 significant epigenetic modifying compounds

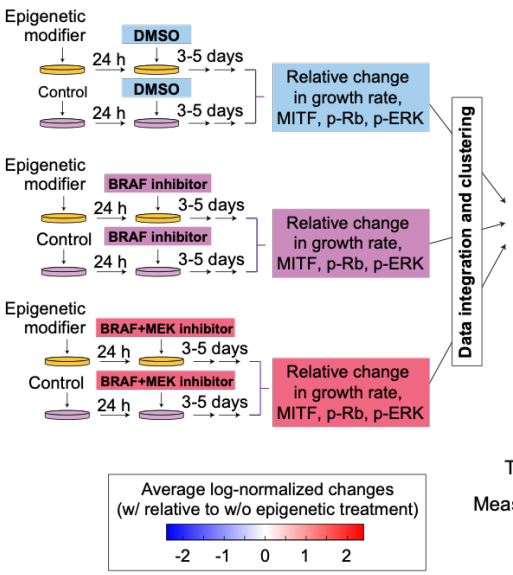

Differential regulation of cellular responses to epigenetic modifying compounds

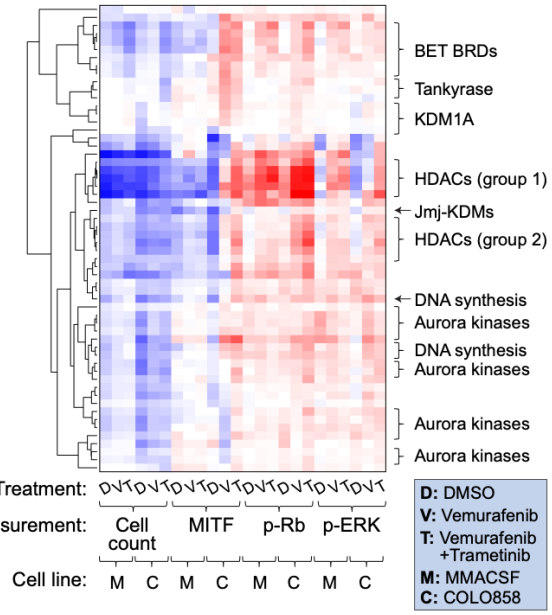

Figure 3

a

2nd stage epigenetic screen

Compound	Target
Givinostat	HDAC
CUDC-907	HDAC
JIB-04	Jmj-KDM
AZ6102	Tankyrase
I-BET-762	BET
OTX015	BET
SP2509	KDM1A

b

Normalized growth rates

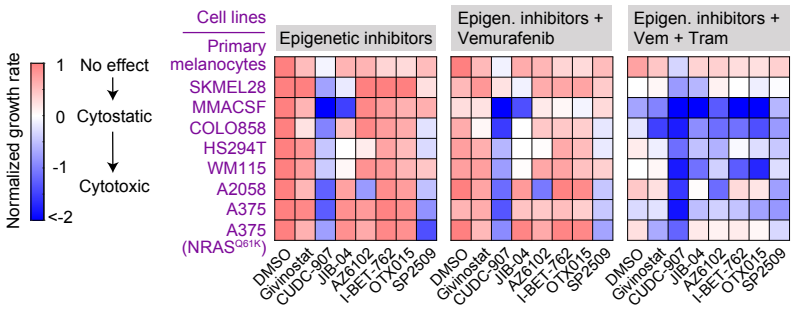

c

Drug combination effectiveness based on the Highest Single Agent model

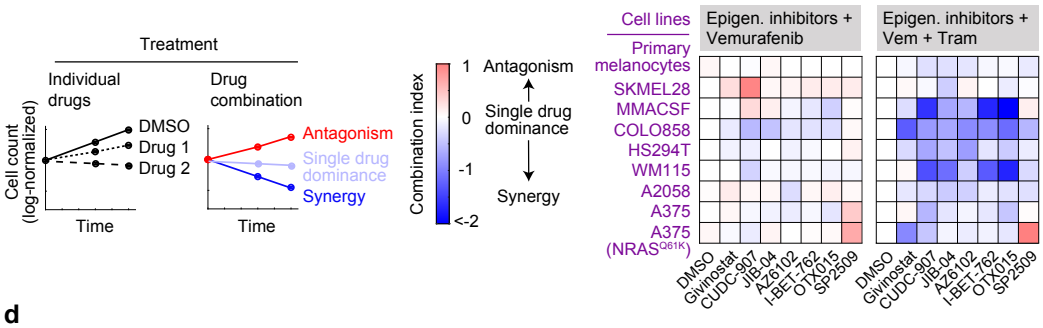

d

Pairwise correlated patterns of drug response (normalized growth rates across 8 cell lines)

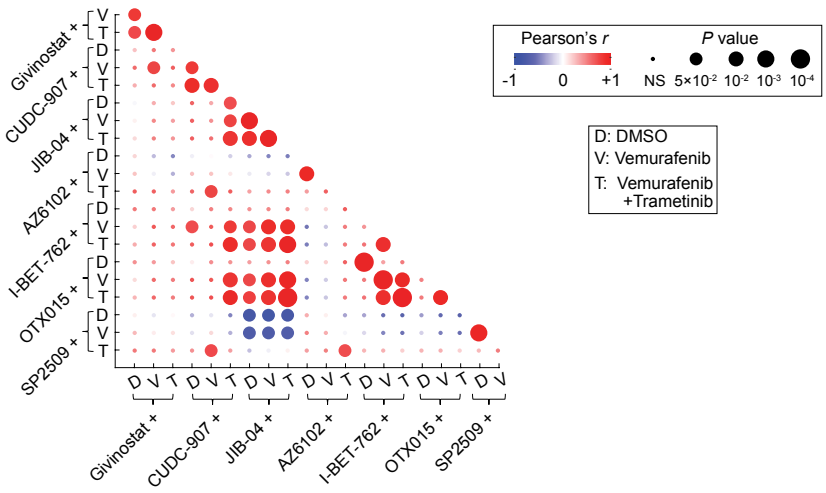

Figure 4

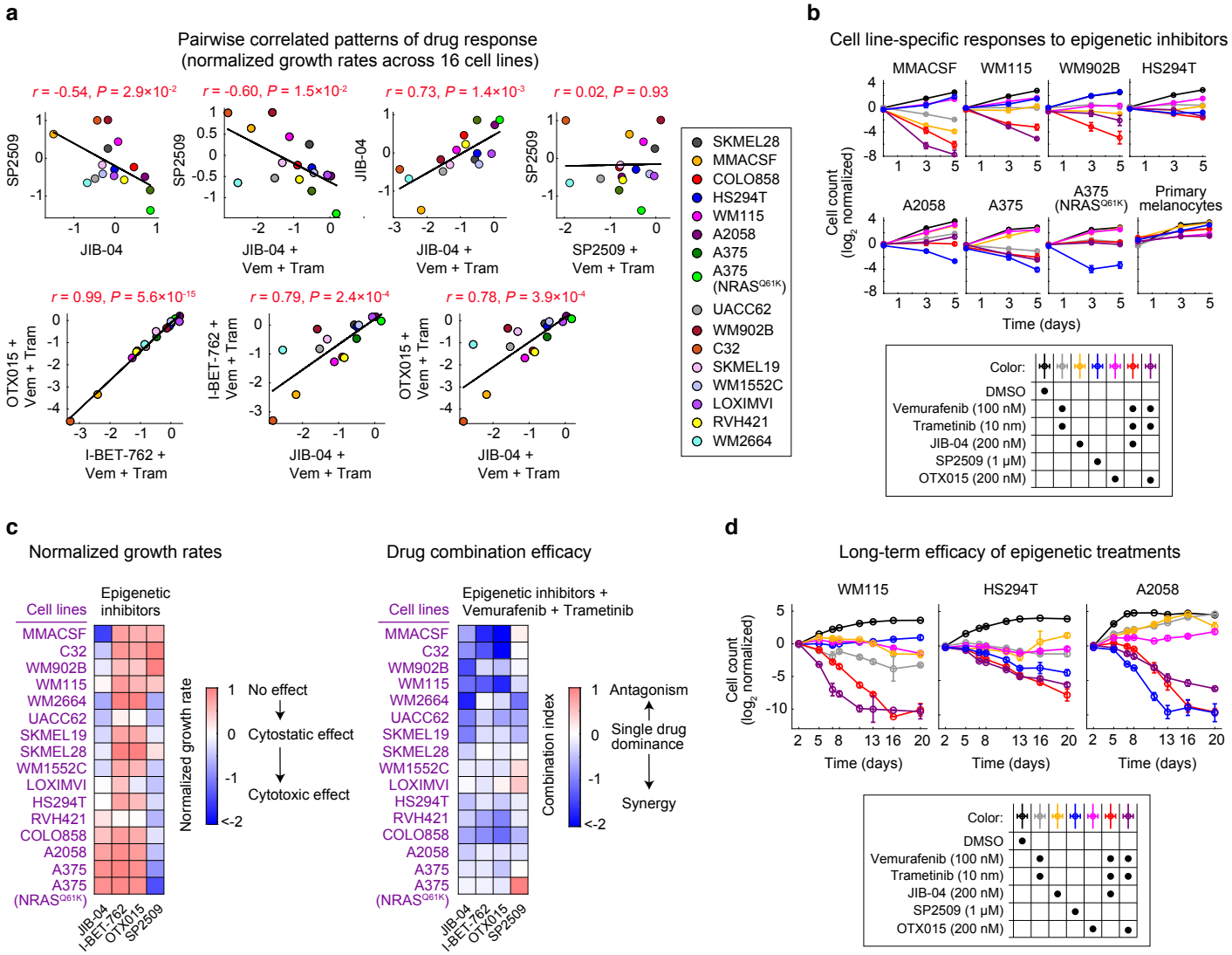
a
Pairwise correlated patterns of drug response
(normalized growth rates across 16 cell lines)
r = -0.54, P = 2.9×10-2
r = -0.60, P = 1.5×10-2
r = 0.73, P = 1.4×10-3
r = 0.02, P = 0.93
SP2509
JIB-04
JIB-04 + Vem + Tram
SP2509 + Vem + Tram
r = 0.99, P = 5.6×10-15
r = 0.79, P = 2.4×10-4
r = 0.78, P = 3.9×10-4
OTX015 + Vem + Tram
I-BET-762 + Vem + Tram
SKMEL28
MMACSF
COLO858
HS294T
WM115
A2058
A375
A375 (NRASQ61K)
UACC62
WM902B
C32
SKMEL19
WM1552C
LOXIMVI
RVH421
WM2664
b
Cell line-specific responses to epigenetic inhibitors
MMACSF
WM115
WM902B
HS294T
A2058
A375
A375 (NRASQ61K)
Primary melanocytes
Cell count (log2 normalized)
Time (days)
Color:
DMSO
Vemurafenib (100 nM)
Trametinib (10 nm)
JIB-04 (200 nM)
SP2509 (1 μM)
OTX015 (200 nM)
c
Normalized growth rates
Cell lines
Epigenetic inhibitors
MMACSF
C32
WM902B
WM115
WM2664
UACC62
SKMEL19
SKMEL28
WM1552C
LOXIMVI
HS294T
RVH421
COLO858
A2058
A375
A375 (NRASQ61K)
JIB-04
I-BET-762
OTX015
SP2509
Normalized growth rate
1 No effect
0 Cytostatic effect
-1 Cytotoxic effect
<-2
Drug combination efficacy
Epigenetic inhibitors + Vemurafenib + Trametinib
Combination index
1 Antagonism
0 Single drug dominance
-1 Synergy
<-2
d
Long-term efficacy of epigenetic treatments
WM115
HS294T
A2058
Cell count (log2 normalized)
Time (days)
Color:
DMSO
Vemurafenib (100 nM)
Trametinib (10 nm)
JIB-04 (200 nM)
SP2509 (1 μM)
OTX015 (200 nM)

Figure 5

a

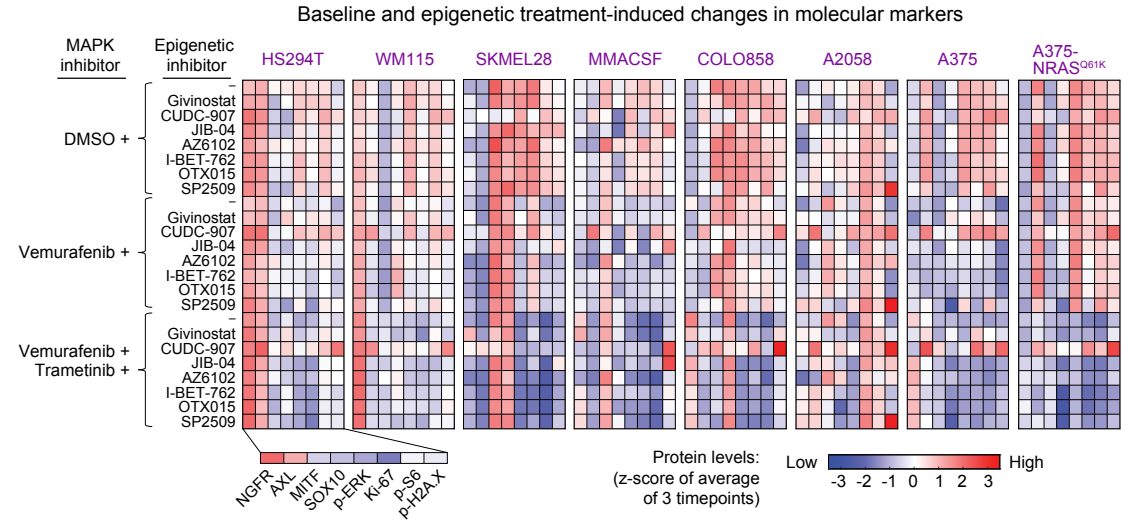

b

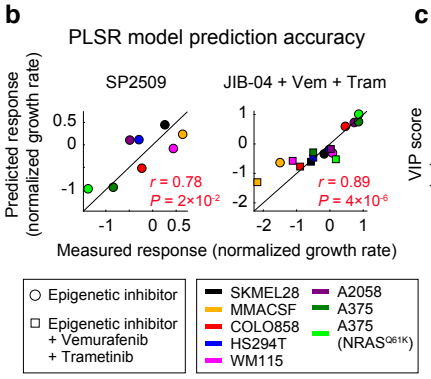

c

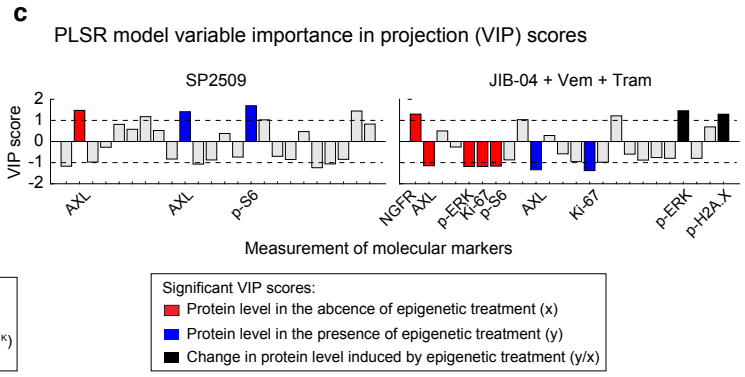

d Correlations between treatment efficacy and single-cell heterogeneity in differentiation state (across 16 cell lines)

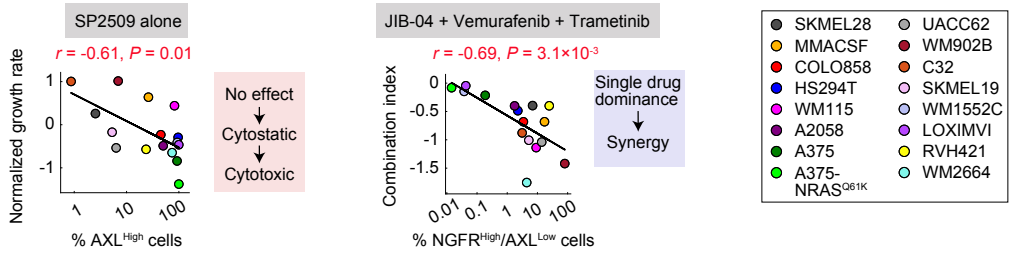

Figure 6

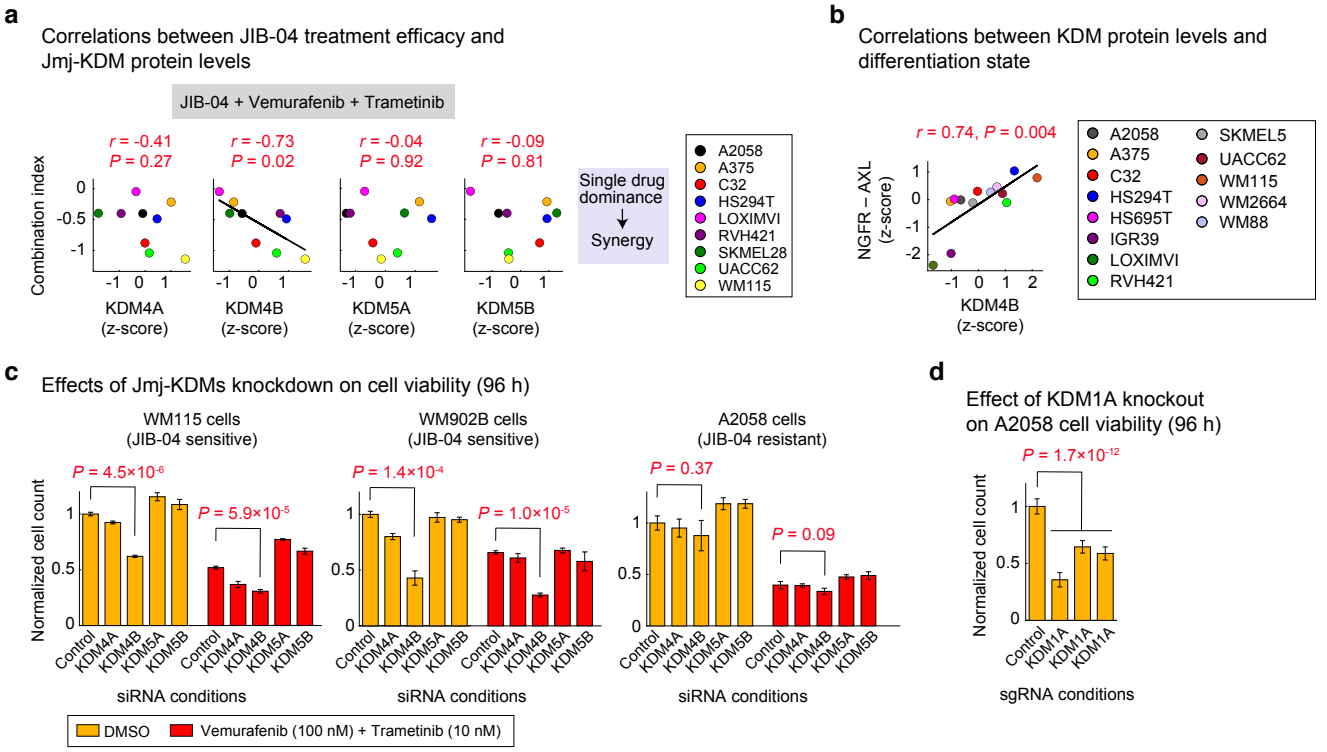
a
Correlations between JIB-04 treatment efficacy and Jmj-KDM protein levels
JIB-04 + Vemurafenib + Trametinib
r = -0.41 P = 0.27
r = -0.73 P = 0.02
r = -0.04 P = 0.92
r = -0.09 P = 0.81
Combination index
KDM4A (z-score)
KDM4B (z-score)
KDM5A (z-score)
KDM5B (z-score)
Single drug dominance
Synergy
A2058
A375
C32
HS294T
LOXIMVI
RVH421
SKMEL28
UACC62
WM115
b
Correlations between KDM protein levels and differentiation state
r = 0.74, P = 0.004
NGFR – AXL (z-score)
KDM4B (z-score)
A2058
A375
C32
HS294T
HS695T
IGR39
LOXIMVI
RVH421
SKMEL5
UACC62
WM115
WM2664
WM88
c
Effects of Jmj-KDMs knockdown on cell viability (96 h)
WM115 cells (JIB-04 sensitive)
WM902B cells (JIB-04 sensitive)
A2058 cells (JIB-04 resistant)
P = 4.5×10-6
P = 5.9×10-5
P = 1.4×10-4
P = 1.0×10-5
P = 0.37
P = 0.09
Normalized cell count
Control
KDM4A
KDM4B
KDM5A
KDM5B
siRNA conditions
DMSO
Vemurafenib (100 nM) + Trametinib (10 nM)
d
Effect of KDM1A knockout on A2058 cell viability (96 h)
P = 1.7×10-12
Normalized cell count
Control
KDM1A
sgRNA conditions
e
Correlations between SP2509 treatment efficacy and protein levels
SP2509 alone
r = -0.42 P = 0.27
r = -0.54 P = 0.13
r = -0.67 P = 0.04
Normalized growth rate
KDM1A (z-score)
ZNF217 (z-score)
KDM1A + ZNF217 (z-score)
No effect
Cytostatic
Cytotoxic
A2058
A375
C32
HS294T
LOXIMVI
RVH421
SKMEL28
UACC62
WM115
f
Correlations between KDM protein levels and differentiation state
r = 0.61, P = 0.01
AXL (z-score)
KDM1A + ZNF217 (z-score)
A101D
A2058
A375
C32
HS294T
HS695T
IGR37
IGR39
LOXIMVI
RPMI7951
RVH421
SKMEL5
UACC62
WM115
WM2664
WM88

Supplementary Figure 1

a

Time-dependent changes in growth rate in response to BRAF/MEK inhibitor treatment

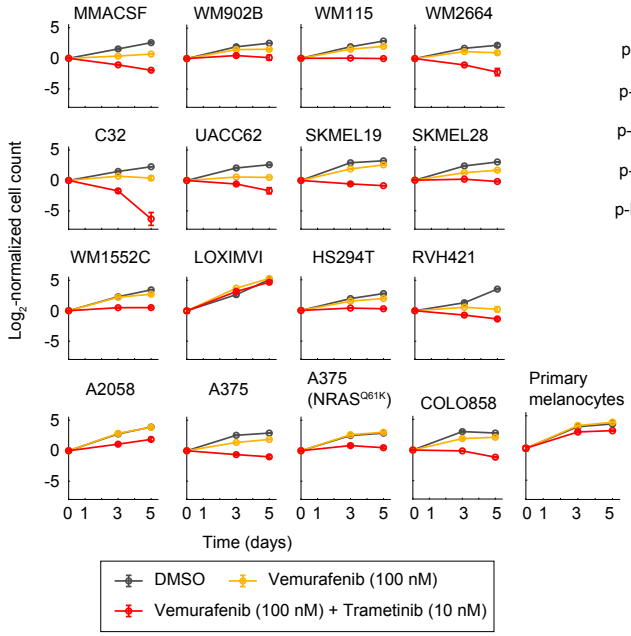

b

Pairwise correlations between fractions of cells in different states (across 16 BRAF-mutant cell lines)

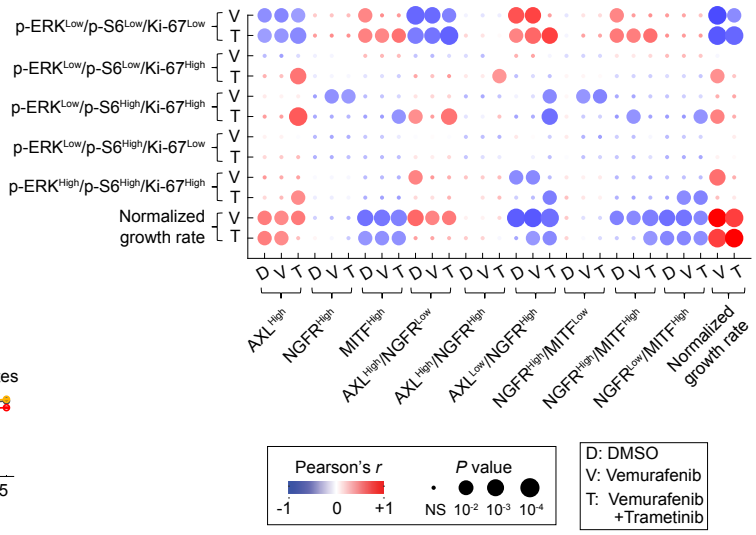

Supplementary Figure 2

Changes in MMACSF cellular growth rate induced by epigenetic treatments

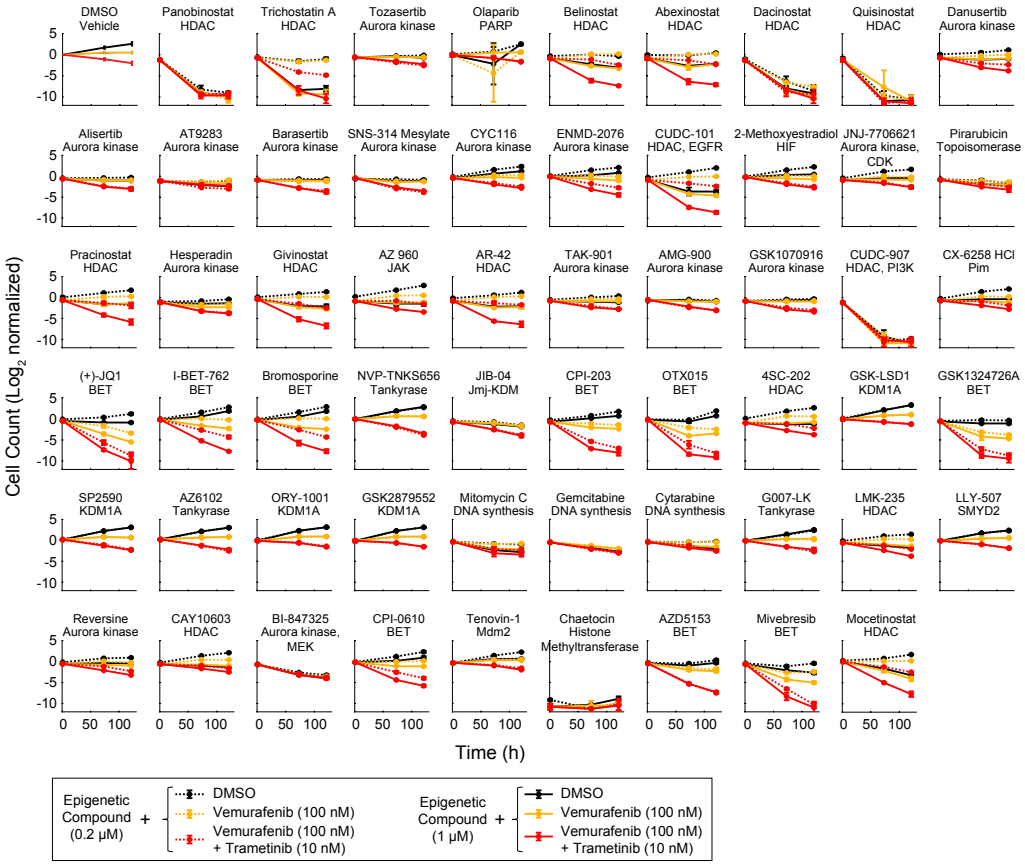

Supplementary Figure 3

Changes in COLO858 cellular growth rate induced by epigenetic treatments

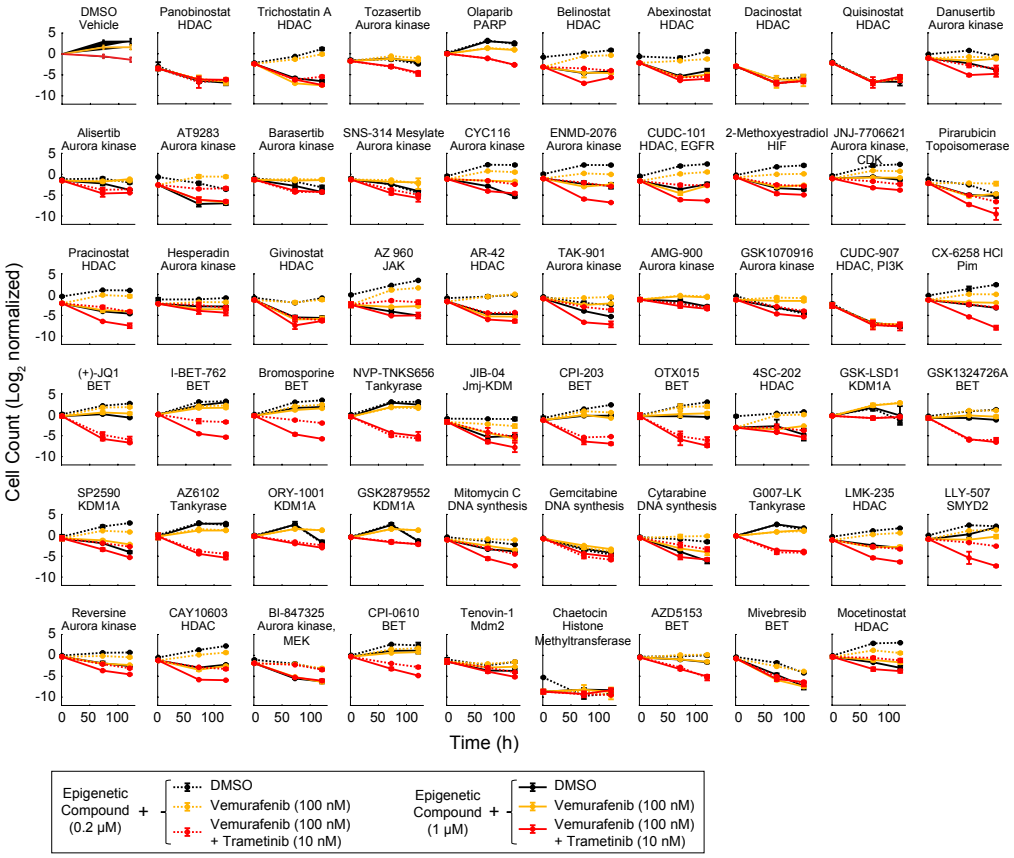

Supplementary Figure 4

a

Differential regulation of cellular states by epigenetic inhibitors

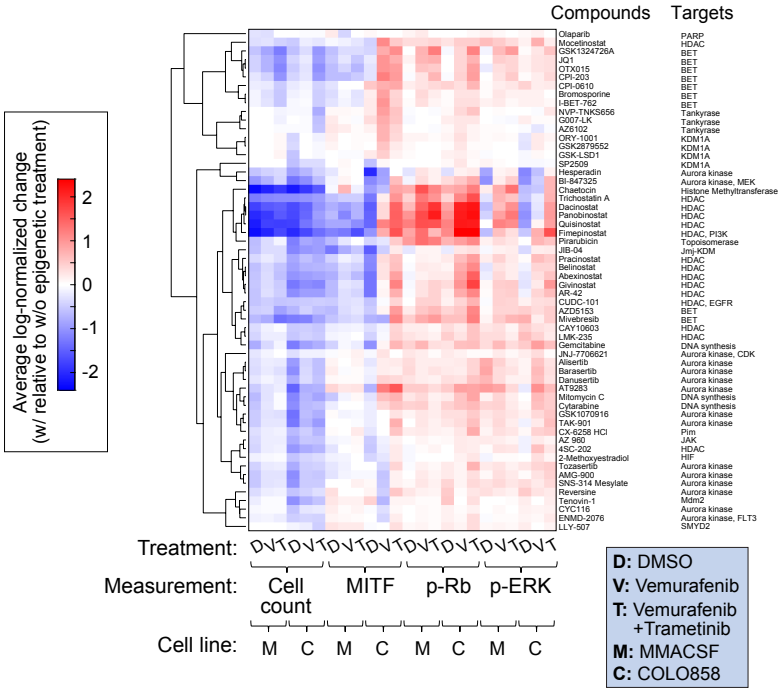

b

Cell line-specific changes in growth rate induced by epigenetic treatments

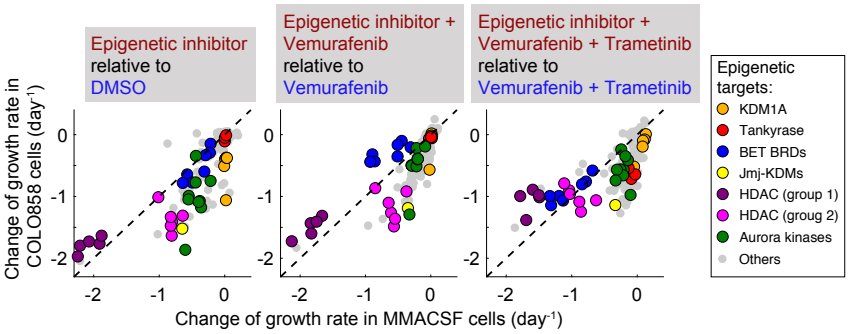

Supplementary Figure 5

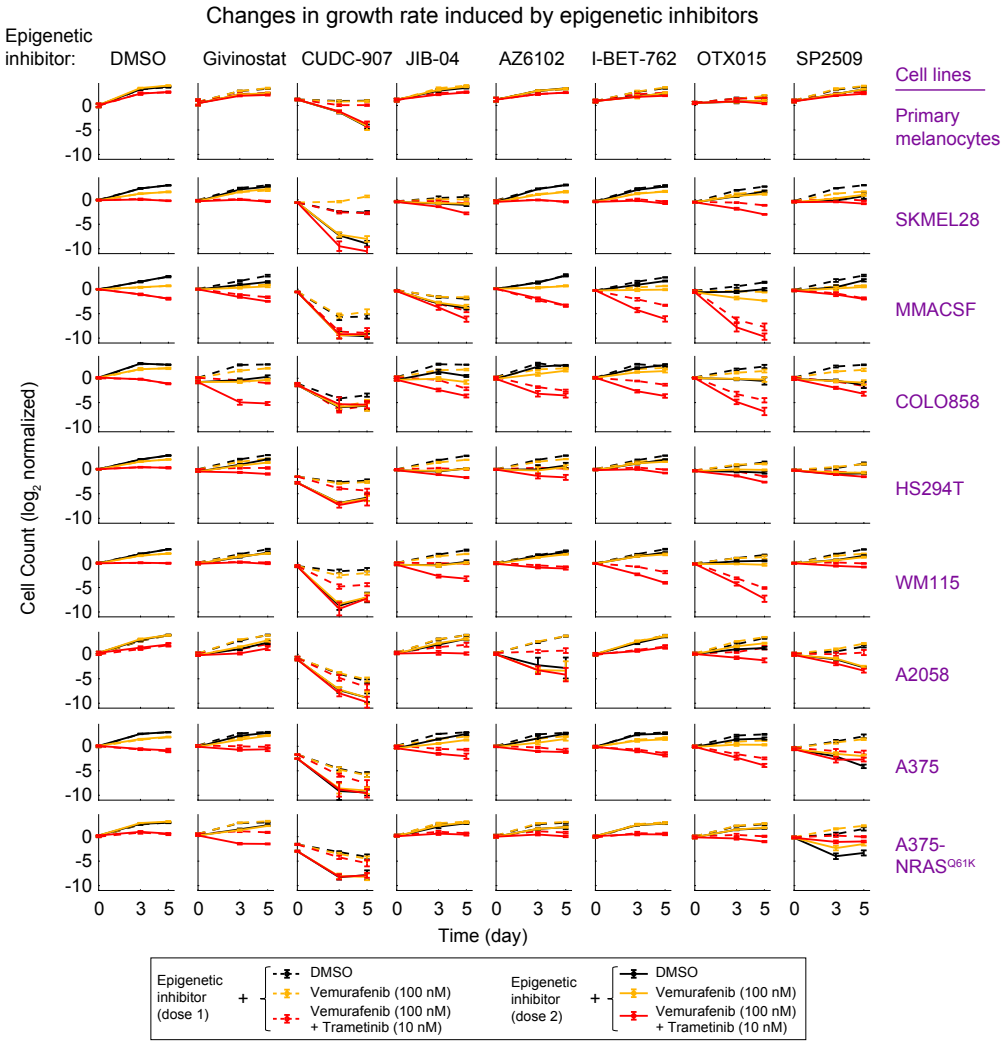

Supplementary Figure 6

a

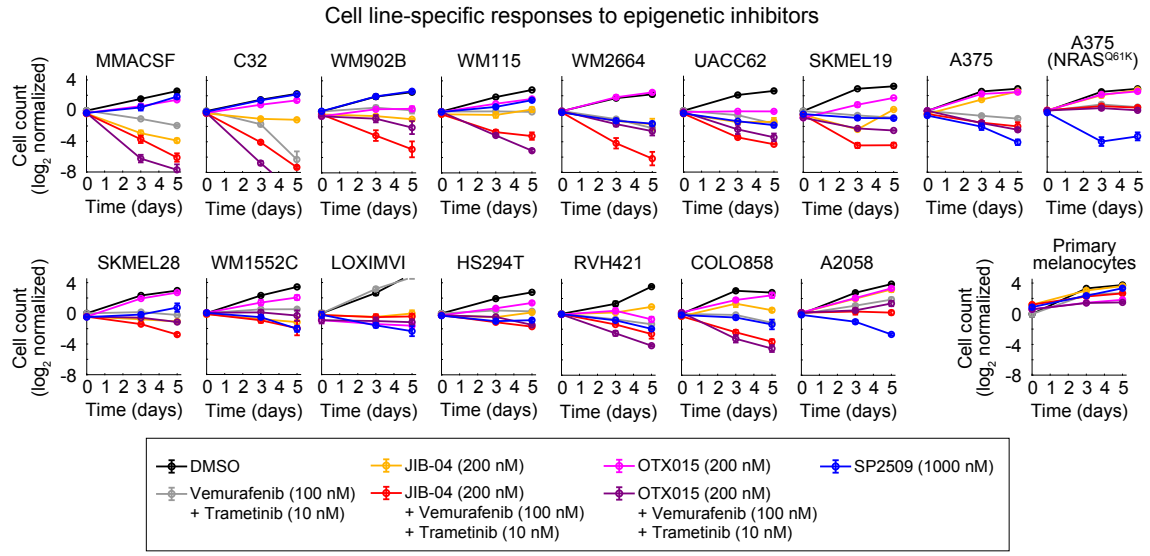

b

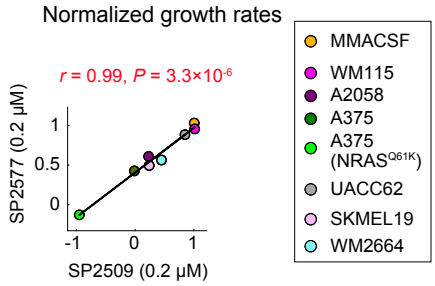

c

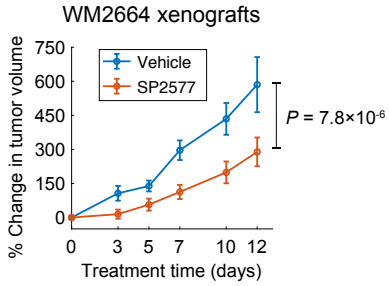

d

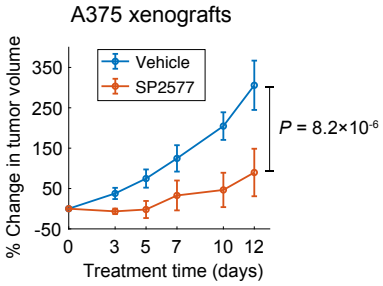

Supplementary Figure 7

a

Performance of PLSR models of epigenetic treatment efficacy

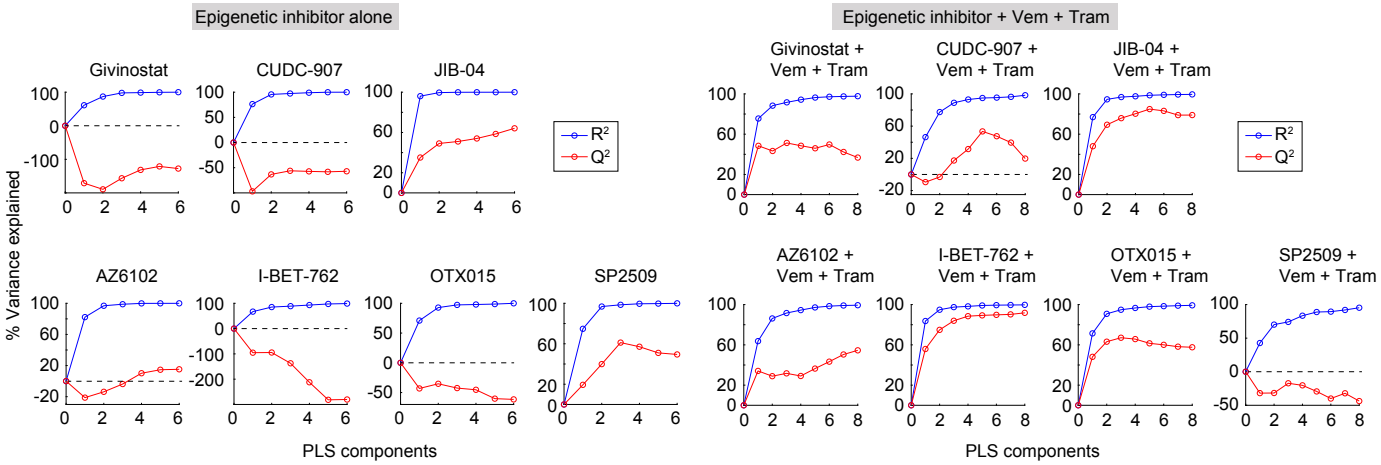

b

Prediction accuracy of PLSR models for BET inhibitors

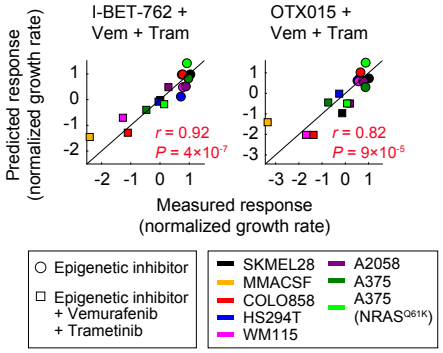

c

Variable importance in projection (VIP) scores of PLSR models for BET inhibitors

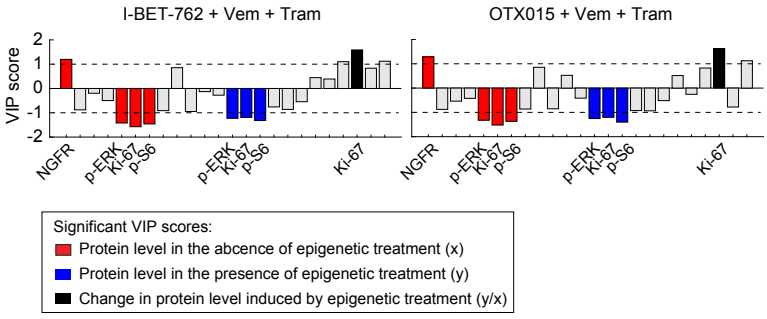

d

Correlations between treatment efficacy and single-cell heterogeneity in differentiation state (across 16 cell lines)

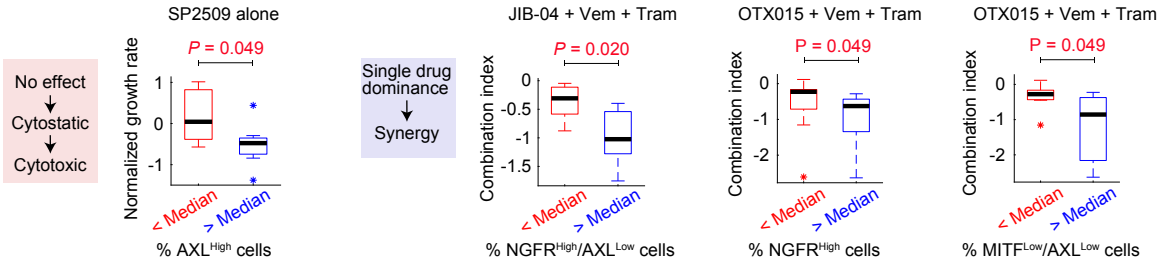

Supplementary Figure 8

a

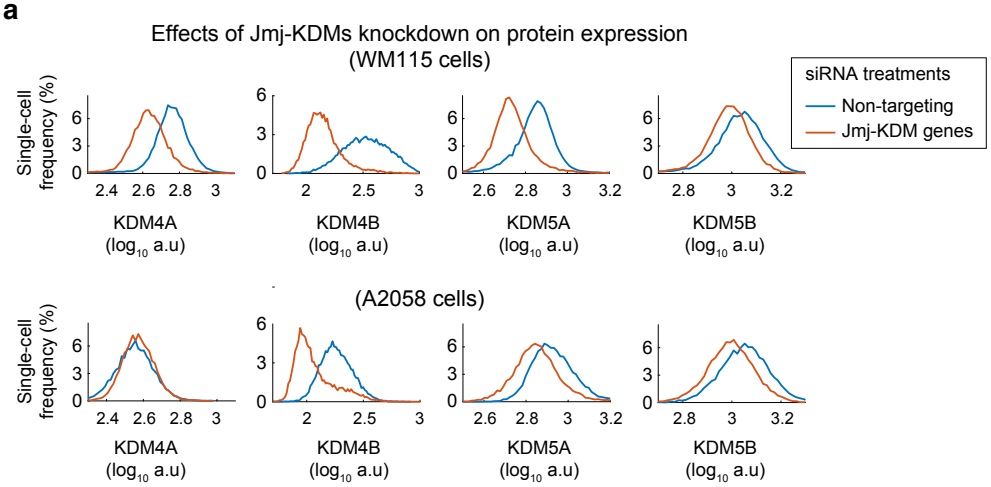
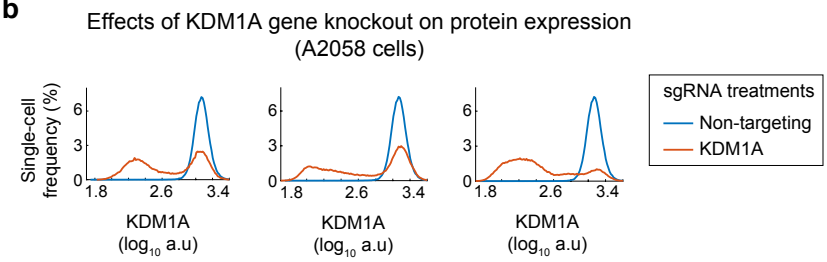
b